



Article

Endohedral Gd-Containing Fullerenol: Toxicity, Antioxidant Activity, and Regulation of Reactive Oxygen Species in Cellular and Enzymatic Systems

Ekaterina S. Sushko ^{1,2,*} , Natalia G. Vnukova ^{2,3}, Grigoriy N. Churilov ^{2,3} and Nadezhda S. Kudryasheva ^{1,3}

¹ Institute of Biophysics SB RAS, Federal Research Center “Krasnoyarsk Science Center SB RAS, 660036 Krasnoyarsk, Russia; n-qdr@yandex.ru

² Institute of Physics SB RAS, Federal Research Center “Krasnoyarsk Science Center SB RAS, 660036 Krasnoyarsk, Russia; nata_hd@rambler.ru (N.G.V.); churilov@iph.krasn.ru (G.N.C.)

³ Siberian Federal University, 660041 Krasnoyarsk, Russia

* Correspondence: kkoval@yandex.ru; Tel.: +7-3912-494-242

Abstract: The Gd-containing metallofullerene derivatives are perspective magnetic resonance imaging contrast agents. We studied the bioeffects of a water-soluble fullerene derivative, gadolinium-endohedral fullerenol, with 40–42 oxygen groups (Gd@Fln). Bioluminescent cellular and enzymatic assays were applied to monitor toxicity and antioxidant activity of Gd@Fln in model solutions; bioluminescence was applied as a signaling physiological parameter. The Gd@Fln inhibited bioluminescence at high concentrations ($>2 \cdot 10^{-1}$ gL⁻¹), revealing lower toxicity as compared to the previously studied fullerenols. Efficient activation of bioluminescence (up to almost 100%) and consumption of reactive oxygen species (ROS) in bacterial suspension were observed under low-concentration exposure to Gd@Fln (10^{-3} – $2 \cdot 10^{-1}$ gL⁻¹). Antioxidant capability of Gd@Fln was studied under conditions of model oxidative stress (i.e., solutions of model organic and inorganic oxidizers); antioxidant coefficients of Gd@Fln were determined at different concentrations and times of exposure. Contents of ROS were evaluated and correlations with toxicity/antioxidant coefficients were determined. The bioeffects of Gd@Fln were explained by hydrophobic interactions, electron affinity, and disturbing of ROS balance in the bioluminescence systems. The results contribute to understanding the molecular mechanism of “hormetic” cellular responses. Advantages of the bioluminescence assays to compare bioeffects of fullerenols based on their structural characteristics were demonstrated.

Keywords: endohedral fullerenol; gadolinium; toxicity; oxidative stress; antioxidant activity; reactive oxygen species; bioluminescence bioassay; hormesis



Citation: Sushko, E.S.; Vnukova, N.G.; Churilov, G.N.; Kudryasheva, N.S. Endohedral Gd-Containing Fullerenol: Toxicity, Antioxidant Activity, and Regulation of Reactive Oxygen Species in Cellular and Enzymatic Systems. *Int. J. Mol. Sci.* **2022**, *23*, 5152. <https://doi.org/10.3390/ijms23095152>

Academic Editor: Narimantas K. Cenys

Received: 17 March 2022

Accepted: 30 April 2022

Published: 5 May 2022

Publisher’s Note: MDPI stays neutral with regard to jurisdictional claims in published maps and institutional affiliations.



Copyright: © 2022 by the authors. Licensee MDPI, Basel, Switzerland. This article is an open access article distributed under the terms and conditions of the Creative Commons Attribution (CC BY) license (<https://creativecommons.org/licenses/by/4.0/>).

1. Introduction

Carbon nano-objects are of great interest for different fields of medicine, pharmacology, and biotechnology due to their specific biological activity [1–3]. Fullerenes are carbon nanomaterials known for their unique cage structure. Numerous fullerene-based compounds with different biological targets have been synthesized; biomedical and bioengineering aspects for their application are currently under intensive review [4–10]. Fullerenes and their derivatives are prospective candidates for anticancer or antimicrobial therapy, cytoprotection, enzyme inhibition, controlled drug delivery, contrast-based or radioactivity-based diagnostic imaging, radio-protection, photosensitization, and biomimetics. Fullerene properties such as antioxidant or pro-oxidant potential, toxicity, membranotropicity, protein-binding affinity, and antiviral, antimicrobial, and anti-apoptotic ability are currently under investigation. It is known [11] that the chemical structure of fullerene derivatives allows them to neutralize reactive oxygen species effectively. This process can occur place in

all media: solutions of low-molecular-weight and high-molecular-weight compounds, biomolecules, cells, and tissues.

Fullerenols are water-soluble polyhydroxylated derivatives of fullerenes. Similar to fullerenes, fullerenols are electron-deficient structures and this property makes them efficient catalyzers in biochemical reactions, as well as prospective pharmaceutical drugs. Additionally, fullerenols are amphiphilic structures: fragments of fullerene skeleton provide them with affinity to hydrophobic fragments of enzymes and lipid structures of cellular membranes, while the hydroxyl groups, with aqueous solubility [1,2]. Hydroxyl substituents distort the π -electron system conjugation of the fullerene skeleton, change the electron-acceptor ability of nanoparticles and can therefore affect their catalytic activity. Hence, the variation of the number of the hydroxyl substituents in the fullereneol structures can change the toxicity and antioxidant activity of the fullereneol nanoparticles.

The amphiphilic properties and electron-acceptor ability provide a wide range of biological effects of the fullerenols: from neutralization of free radicals [12] to cell protection and drug transportation [1,12–14]. The antioxidant properties endow fullerenols with the ability to neutralize reactive oxygen and nitrogen species [15–19], and to function as radioprotectors [17], antitumor [20], or neurological [12,17–19] drugs. The biological activity of C_{60} -fullerenols with different number of hydroxyl groups have been intensively studied over the past decades [12–16]. Toxic and antioxidant effects of the fullerenols are revealed.

It is known that gadolinium-based preparations have potential in magnetic resonance imaging and cancer research due to unique paramagnetic properties of gadolinium [21,22]. The most medically used gadolinium-containing compounds are gadodiamide, gadopentetate dimeglumine, gadoterate meglumine, etc. [23,24]; however, there are concerns that these substances may be toxic [24]. They are known to lead to severe skin and systemic diseases (gadolinium ions can exhibit neurological and cardiovascular toxicity [25]), renal dysfunction [26], and intracranial deposition of gadolinium [27]. The problem of toxicity of gadolinium preparations can be solved by involvement of gadolinium into the fullerene carcass. $Gd@C_{82}$ is a common gadolinium metallofullerene (gadofullerene), consisting of a core of a gadolinium (Gd) atom and a closed outer shell of 82 carbon atoms [28,29]. It is supposed [21,30–38] that an endohedral fullerene complex and its derivatives can be widely used in biomedicine as novel magnetic resonance imaging (MRI) contrast agents. The high electron affinity of $Gd@C_{82}$ suggests its ionic structure, in which the inner paramagnetic metal ion Gd^{3+} is encapsulated in the negatively charged carbon cage, thus forming a dipole charge-transfer complex $Gd^{3+}@C_{82}^{3-}$, which prevents a release of toxic ions Gd^{3+} into the bioenvironment [34]. Ionic conjecture for $Gd@C_{82}$ is widely accepted by the scientific community [30].

Endohedral Gd-containing fullerenols, water-soluble derivatives of $Gd@C_{82}$, are good candidates for biomedical applications due to their solubility in water. It is shown that they improve the effectiveness of cancer therapy in combination with chemotherapy [39].

Bioluminescence-based assays are appropriate candidates to study the biological activity of fullerene derivatives due to their simplicity, sensitivity, and high rates of analysis (1–20 min). The bioluminescent assays use the luminescence intensity as a physiological testing parameter; this parameter can easily be measured using simple physical devices. These advantages allow investigators to conduct a large number of tests under comparable conditions during a short time-period; therefore, these tests are adapted to extensive statistical processing, particularly, at low-concentration (low-intensity or low-dose) exposures, which usually produce “noisy” responses and they are described in terms of “stochasticity”.

The bioluminescence bacteria-based assay is commonly used; it has been applied for more than fifty years to monitor the “general” toxicity of complex media [40–44]. The use of the bioluminescence enzymatic assay is a relatively new direction in the toxicology practice [45,46]. As a rule, the enzymatic bioluminescent assay is based on two coupled enzymatic reactions of luminous bacteria (presented in Section 3.2). We used this assay to assess two toxicity types—“general” and “oxidative” ones. The “general” toxicity type integrates all the interactions of the bioluminescent assay system with toxic compounds:

redox processes, polar and non-polar binding, etc.; it uses the bioluminescence intensity as a testing parameter. The “oxidative” toxicity type is attributed to the redox properties of toxic compounds only; it uses another testing kinetic parameter—the bioluminescence delay period [47]. The differences in “general” and “oxidative” toxicity evidence the involvement of the hydrophobic (non-polar) interactions in the toxic effect.

Previously [48–51], we suggested an original bioluminescence-based method to evaluate antioxidant properties of bioactive compounds. The method involved (1) application of model solutions of oxidizers to produce an “artificial oxidation stress” on luminous bacteria (or their enzyme systems); (2) evaluation of the toxic effect of the model oxidizer solutions on the bioassay systems; (3) exposition of the oxidizer solutions to the bioactive compounds and evaluation of changes in the toxicity (i.e., detoxification of the model oxidizer solutions or, in other words, “antioxidant” effect); (4) calculation of coefficients of antioxidant activity of the bioactive compounds. As we can use the cellular (luminous bacteria) or enzymatic (bacterial enzymes) bioassay systems, we can compare the antioxidant effects at cellular and enzymatic levels. Additionally, differences in the “general” and “oxidative” toxicity provide information on the amphiphilic properties of the bioactive compounds.

Humic substances, products of natural decomposition of organic matter in soils, coals, and bottom sediments, were the first bioactive compounds that we studied using this approach [49–51]. Later, the bioeffects of gold nanoparticles were analyzed in [52], the toxicity and antioxidant activity of a series of different fullereneol nanoparticles were evaluated and compared in [53–59], prooxidant properties of mignette nanoparticles were demonstrated [60]. Thus, we have demonstrated that bacteria-based and enzyme-based bioluminescence assays exhibit strong potential as appropriate tools for studying and comparing the bioeffects of nanocompounds of different structures.

The question arises: does the involvement of the gadolinium atom to the fullerene cage change the toxicity and antioxidant activity of fullereneol? Recent theoretical calculations [61] predicted that the Gd atom promotes the chemical reactivity and electrophilic properties of fullereneol cages. It was shown in [6–9] that electron affinity and average polarizability of Gd@C₈₂ are more significant than those for pristine fullerenes [62–65]; hence, it is a stronger electron donor and acceptor. Therefore, the fullereneol can act an efficient antioxidant in addition to its application as an MRI contrast agent.

Antioxidant properties of bioactive compounds are supposed to be concerned with reactive oxygen species (ROS) in biological systems. The correlations between the ROS content and the toxic/antioxidant effects of bioactive compounds (fullerenols, gold nanoparticles, and radionuclides) in suspensions of luminous marine bacteria were studied in [52,53,59,66–69]. The role of ROS in the toxic and antioxidant effects of endohedral Gd-containing fullerenols is of high interest; it has not been studied experimentally yet.

In this work, we studied the toxic and antioxidant properties of the endohedral fullereneol Gd@C₈₂O_x(OH)_y, where $x + y = 40–42$, which is further referred to as Gd@Fln. The bacteria-based and enzyme-based bioluminescence assays were used to evaluate toxic and antioxidant characteristics of Gd@Fln. The toxic characteristics of Gd@Fln were determined in high-concentration ranges; the low-concentration activation effects of Gd@Fln were found. The bioeffects of Gd@Fln were compared to those of other fullerenols studied earlier. Correlations between the ROS content and the toxic/activating characteristics of Gd@Fln were found in different Gd@Fln concentration ranges. The conditions of model oxidative stress (i.e., solutions of model oxidizers of organic and inorganic types) were applied to evaluate the antioxidant coefficients of Gd@Fln; they were determined at different concentrations and times of exposure to Gd@Fln. Correlations between the antioxidant coefficients and the ROS content were found and discussed. The role of hydrophobic interactions, electron affinity and ROS consumption in the bioeffects of Gd@Fln were taken into consideration. Additionally, in Section 2.2.3 we elucidate the conditions of oxidative stress; the section compares the ROS content in oxidizer solutions in the absence and presence of the biological structures (cells and enzymes).

2. Results and Discussion

2.1. Effects of Gd@Fln on Bioluminescence and ROS Content

We studied the effects of Gd@Fln of different concentrations (10^{-14} – 3 gL^{-1}) on the bioluminescence of bacterial cells and enzymatic systems.

Figure 1A presents a dependence of the relative bioluminescent intensity (I^{rel} , Equation (1), Section 3.2) of luminous bacterial suspensions (curve 1) and enzymatic system (curve 2) on the concentration of Gd@Fln, at initial time of exposure to Gd@Fln (5-min).

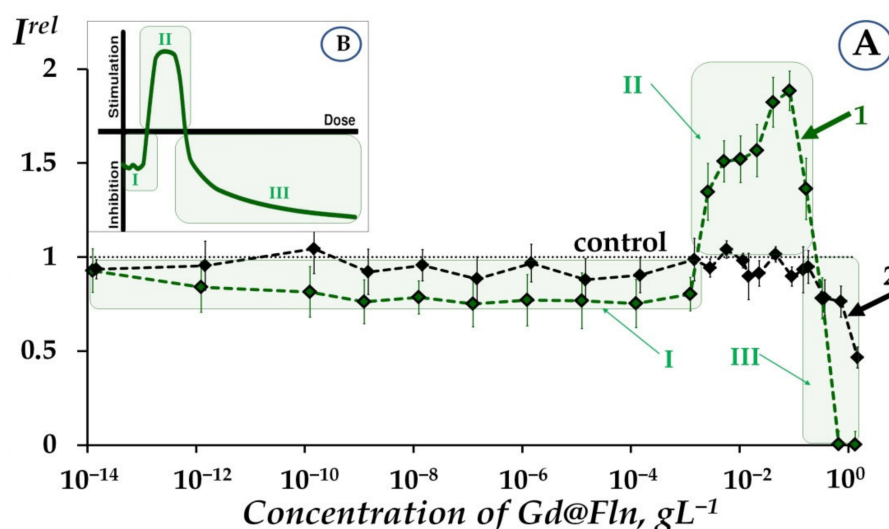


Figure 1. (A) Relative bioluminescence intensity, I^{rel} , at different concentrations of fullereneol Gd@Fln in bacterial suspension (1) and enzymatic system (2). The 5-min exposure. (B). Scheme of hormesis dose-effect model is presented according to [67]. Hormetic stages: I—stress recognition, II—physiological activation, III—inhibition of vital functions. “Control” corresponds to the absence of Gd@Fln in the experimental solutions.

It is seen from Figure 1A that dependence of I^{rel} on fullereneol concentration in bacterial suspension (curve 1) includes three stages: (I) moderate inhibition ($I^{rel} < 1$) at 10^{-14} – 10^{-3} gL^{-1} , (II) activation ($I^{rel} > 1$) at 10^{-3} – $2 \cdot 10^{-1} \text{ gL}^{-1}$, and (III) inhibition ($I^{rel} < 1$) at $2 \cdot 10^{-1}$ – 3 gL^{-1} .

It should be noted that there exists a difference between bioluminescence kinetics under exposure to higher and lower Gd@Fln concentrations. Figure S1 (Supplementary Materials) presents examples of these kinetics. The conventional border between higher and lower concentration ranges was ca. $2 \cdot 10^{-1} \text{ gL}^{-1}$, it was taken into consideration during the course of further data analysis. Studies of higher- and lower-concentration effects of Gd@Fln are presented in Sections 2.1.1 and 2.1.2, respectively.

2.1.1. Toxicity of Gd@Fln via Bioluminescence Enzymatic and Cellular Assays at High-Concentration Ranges

We examined the toxicity factor of fullereneol Gd@Fln using cellular and enzymatic bioluminescence assays. As is evident from Figure 1A, Gd@Fln suppresses bioluminescence of both bacterial and enzymatic systems at high concentrations ($>2 \cdot 10^{-1} \text{ gL}^{-1}$). The suppression is evidence of the fullereneol toxic effect; it is supposed to be concerned with complex multiple processes which resulted in inhibition of membrane and intracellular processes (for bacterial cells) [47,49] or chemical and biochemical reactions (for enzymatic system) by low-molecular and nano- compounds as previously discussed [47,49,54,56,70]. Note, that the inhibition processes are not concerned with the peculiarities of the luminescence registration, since “concentration quenching” resulting from collisional intermolecular interactions was initially excluded (See Section 3.2). The values of EC_{50} for Gd@Fln were determined as 0.46 and 1.4 gL^{-1} for the bacterial suspension and enzymatic system, respectively. It is

evident that the bacterial system revealed higher sensitivity to Gd@Fln (i.e., lower value of EC_{50}), likely due to hydrophobic interactions with cellular membrane involvement. Similar results were observed earlier with other fullerenols of different structures [53] (fullerenol with exohedral iron atom was excluded due to specific action of iron on metabolism of the bacterial cells). The EC_{50} values of fullerenols of different structures were determined earlier under similar conditions; they ranged from 0.003 to 0.031 gL^{-1} for the bacterial suspension [53] and from 0.002 to 0.092 gL^{-1} for the enzymatic system [53,59]. Hence, toxicity of Gd@Fln is lower (i.e., EC_{50} values are higher in both bioluminescent systems) than that of the other fullerenols studied earlier [53,59]. This effect can be explained by larger cage size of Gd@Fln (involving 82 carbon atoms) and its tendency towards aggregation. The aggregate formation was studied in detail in [21,71–73] with the example of endohedral fuller enol with 22 hydroxyl groups, Gd@C₈₂(OH)₂₂; polyanion nano-aggregation into cluster in aqueous solutions was demonstrated. The aggregation might prevent intensive interactions of Gd@Fln with cellular membranes or water-soluble enzymes.

2.1.2. Low-Concentration Effects of Gd@Fln

Bioluminescence activation of bacteria ($I^{rel} > 1$, Figure 1A, curve 1) was found at low-concentration exposure to Gd@Fln (10^{-3} – $2 \cdot 10^{-1}$ gL^{-1}). The activation was significant—up to almost 100%, as compared to control. The bacterial response to Gd@Fln corresponds to the conventional “hormesis” model [74–77], which is presented in Figure 1B. It is known that the model includes, in the broadest case, three stages of the biological dose-dependent response—stress recognition (I), activation (II), and inhibition of organismal functions or toxic effect (III). As a concept, hormesis involves favorable biological responses to low exposures of stressors [78,79].

In contrast to bacteria, enzymatic response to Gd@Fln did not show bioluminescence activation (curve 2, Figure 1A). This is an indication that the bacterial activation (curve 1, Figure 1A) is concerned with indirect effects on bioluminescent reaction and probably related to cell membrane processes with hydrophobic interactions involved.

Previously [53–59], we did not observe low-concentration activation of bacterial bioluminescence by the other fullerenols; only high-concentration inhibition (toxic effect) was found. This difference is likely evidence of higher reactivity and reversible electron-acceptance ability of Gd@Fln [65,80,81]. Previous experimental and theoretical results support this supposition. It was found in [82], that Gd endofullerene is characterized by a significantly (one-and-a-half to two orders of magnitude) higher reactivity with respect to C₆₀ and C₇₀, which can be accounted for by the nonuniform distribution of electron density of the fullerene cage due to the presence of the endohedral atom. The electron affinity of Gd@C₈₂ is more significant than those for pristine C₆₀ and C₇₀ (1.25 and 1.19 times, respectively); the insertion of Gd into a C₈₂ cage increases the electron affinity to 3.3 eV [64]. Gd³⁺@C₈₂³⁻ can be involved in free-radical addition reactions, which can change the electronic structure of the inner cluster and affect its configuration [83].

2.1.3. Involvement of ROS in the Responses of Bacterial and Enzymatic Systems to Gd@Fln

It should be noted that we initially studied time-courses of ROS content in control samples (i.e., without Gd@Fln) of bacterial and enzymatic systems for the time of bioluminescent experiment, 45 min. We found an increase in ROS content (from $1.9 \cdot 10^{-5}$ M to $4.7 \cdot 10^{-5}$ M) in the control enzyme solutions, while the ROS content in the control bacterial suspensions was almost constant—about $4.5 \cdot 10^{-6}$ M. The explanation is likely the following: the increase mentioned can be explained with dark processes associated with the accumulation of peroxide compounds in the reaction of bacterial luciferase [84]. Bacterial cells are likely able to balance ROS content and maintain homeostatic levels of ROS involved in metabolic coupled redox reactions.

In order to verify the role of ROS in the bioeffects of Gd@Fln (Figure 1A), we determined ROS content in bacterial suspensions and enzymatic systems. Dependences of ROS content on time of exposure to fullereneol Gd@Fln were studied at different con-

concentrations of Gd@Fln solutions (10^{-13} – 3 gL^{-1}). Examples of kinetics of relative ROS content, ROS^{rel} , at two concentrations of fullereneol Gd@Fln are presented in Figure S2 (Supplementary Materials).

Values of ROS^{rel} were determined along with I^{rel} in bioluminescence experiments and presented in Figure 2 for bacterial (Figure 2A) and enzymatic (Figure 2B) systems.

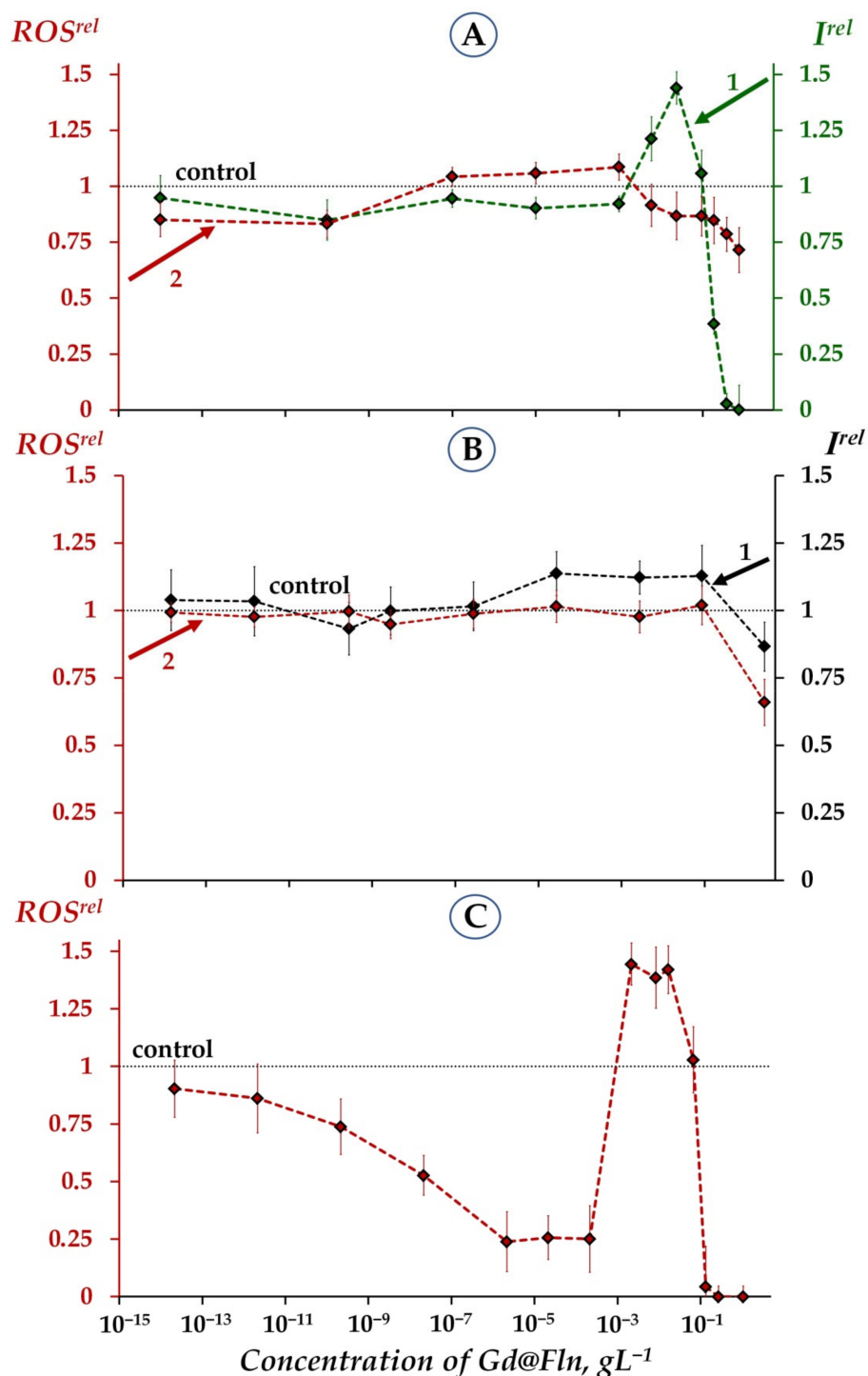


Figure 2. Relative bioluminescence intensity, I^{rel} , (1) and relative ROS content, ROS^{rel} , (2) in bacterial suspension (A), enzymatic system (B) and distilled water (C) at different concentrations of fullereneol Gd@Fln. Time of exposure to Gd@Fln was 1 min. Concentration of ROS in the control bacterial suspension was $\sim 4.5 \cdot 10^{-6}$ M, in the control enzymatic sample— $1.9 \cdot 10^{-5}$ M, in distilled water— $3 \cdot 10^{-7}$ M. “Control” corresponds to the absence of Gd@Fln in the experimental solutions.

We analyzed correlations between concentration dependencies of I^{rel} and ROS^{rel} for bacterial suspensions (Figure 2A) in a low-concentration range of Gd@Fln: 10^{-7} – 10^{-1} gL $^{-1}$. This range revealed a negative correlation ($r = -0.8$, $p < 0.05$) and therefore demonstrated the inverse dependence between bioluminescence intensity and ROS content. We can conclude that the bacterial bioluminescence activation by Gd@Fln ($I^{rel} > 1$, curve 1, Figure 2A) is related to the moderate decrease in ROS ($ROS^{rel} < 1$, curve 2, Figure 2A), probably as a result of intensification of ROS consumption by the bacteria induced by fullereneol [84,85]. This conclusion infers the molecular mechanism of “hormetic” response of the bacterial cells to fullereneol. A higher concentration range of Gd@Fln (10^{-1} – $8 \cdot 10^{-1}$ gL $^{-1}$) revealed a positive correlation between concentration dependencies of I^{rel} and ROS content ($r = 0.8$, $p < 0.05$). This result reveals different molecular mechanisms of Gd@Fln influence on bacteria at lower-concentration and higher-concentration ranges, resulting in bioluminescence activation and inhibition, respectively. Inhibition and activation of bacterial bioluminescence intensity by ROS was reported previously for bacterial and enzymatic assays, hydrogen peroxide was applied by the authors as a representative of ROS [86,87].

Figure 2B presents the dependences of I^{rel} and ROS^{rel} on concentrations of Gd@Fln in the enzymatic system (curves 1 and 2, respectively). No reliable bioluminescence activation was observed in the enzyme solutions (curve 1, Figure 2B), similar to the previous results of the analogous experiment presented in Figure 1A, curve 2. A positive correlation ($r = 0.9$, $p < 0.05$, 10^{-7} – 3 gL $^{-1}$) between the concentration dependencies of I^{rel} and ROS^{rel} was found, Figure 2B.

It should be noted that a similar high-concentration decline in both of I^{rel} and ROS^{rel} as well as positive correlation between these parameters were reported earlier for enzymatic system exposed to the other fullereneol (C₆₀) with low number of oxygen substituents [59]. This correlation was suggested to have resulted from the consumption of ROS in the course of the bioluminescence reaction. The physicochemical mechanism of fullereneol’s influence on the enzymatic assay system is likely due to its ability to neutralize free radicals [53] including peroxide radicals. It is known that one of the intermediates of the bioluminescent luciferase reaction (reaction 2, Section 3.2), flavin peroxy-semiacetal [88,89], is a peroxide that is categorized as a ROS. Hence, the decrease in ROS content ($ROS^{rel} < 1$), at high fullereneol concentrations can account for the inhibition of the bioluminescent reaction (reaction 2, Section 3.2). The bacterial bioluminescence reaction can be considered as a model of enzymatic oxygen-dependent reactions taking place in all living organisms.

Hence, intermediate conclusions from the results in Figure 2A,B are the following:

1. Similar to the previous results [53,59], the toxic effects of Gd@Fln can be concerned with the lack of ROS ($ROS^{rel} < 1$) in bacteria-based and enzyme-based assay systems. It takes place at high fullereneol concentrations ($>2 \cdot 10^{-1}$ gL $^{-1}$, Figure 1A).
2. Additionally, a moderate ROS decay ($ROS^{rel} < 1$) at low-concentration fullereneol exposure (10^{-3} gL $^{-1}$ – $2 \cdot 10^{-1}$ gL $^{-1}$) might be related to the activation of bacterial bioluminescence as a result of ROS consumption.

As previously mentioned, it is commonly recognized that only the excess of ROS leads to toxic effects which resulted in DNA damage and cell death [90–92]. Our results develop our understanding of ROS functions in biological systems revealing complex interrelations between ROS content and physiological efficiency. Probably, there exists an optimum range of ROS concentrations, which is balanced naturally by living systems.

Figure 2C presents ROS content in aqueous solutions of Gd@Fln. The complexity of the concentration dependence is evident from this Figure. A low-concentration range ($<10^{-4}$ gL $^{-1}$) shows a decline of ROS content as compared to control ($ROS^{rel} < 1$); hence, this range alone provides antiradical activity of fullereneol. A higher concentration range (10^{-4} – 10^{-1} gL $^{-1}$) demonstrates an increase in ROS content ($ROS^{rel} > 1$). Previously, we did not observe such a distinct increase in ROS content in aqueous solutions of other fullereneols [53]; mechanism of this phenomenon should be further elucidated. However, we can preliminarily suggest that the decay in ROS-neutralizing ability might be concerned with dipole nature of Gd@Fln and formation of aggregates. The high efficiency of aggregate

formation was confirmed previously: it was found that clusters of endohedral metal-fullerenes reach hundreds of nanometers [93,94], in contrast to tens-nanometer clusters of empty fullerenes [95].

Nevertheless, it is seen that the discussed concentration range with high ROS content (10^{-4} – 10^{-1} gL $^{-1}$, Figure 2C) provides the bioluminescence activation, noticeable or slight for bacteria (Figures 1 and 2A curves 1) or enzymes (Figure 2B, curve 1), respectively, with ROS^{rel} -values closed to control (Figure 2A,B, curves 2). The supposition can be made that biological structures, cellular or enzymatic, mitigate deviations of ROS content in environment via intensification of the bioluminescence function. In previous works, the detoxification of reactive oxygen by luciferase reaction was discussed in [96]; in classic work by Wilson and Hastings [97], authors stated that luciferase “transforms excess energy . . . into light energy instead of being all lost as heat”.

2.2. Antioxidant Activity of Fullerenol and ROS Content

To study antioxidant activity of fullerenol Gd@Flu, we excluded a high-concentration range of Gd@Flu inhibiting bioluminescence ($>2 \cdot 10^{-1}$ gL $^{-1}$ for both bacterial and enzymatic systems) based on the results presented in Section 2.1.1, Figure 1A.

Antioxidant activity of fullerenol Gd@Flu was studied under conditions of model oxidative stress, i.e., in model solutions of oxidizers of organic and inorganic types (1,4-benzoquinone and potassium ferricyanide $K_3[Fe(CN)_6]$, respectively). We “fixed” conditions of model oxidative stress by using the effective concentrations of oxidizers, EC_{50} ; values of EC_{50} are presented in Section 3.2. Bioluminescence intensity of the bacterial and enzymatic systems was measured in the absence and presence of Gd@Flu under conditions of the model oxidative stress; concentrations of Gd@Flu were varied. Antioxidant coefficients of I^{rel}_{Ox} and T^{rel}_{Ox} were calculated and compared to ROS content. Values of $I^{rel}_{Ox} > 1$ and $T^{rel}_{Ox} > 1$ were evidence of antioxidant activity of Gd@Flu.

2.2.1. Antioxidant Coefficients I^{rel}_{Ox} and ROS Content

Antioxidant coefficients I^{rel}_{Ox} (Equation (3), Section 3.2) and relative ROS content, ROS^{rel}_{Ox} , were calculated in a wide range of Gd@Flu concentrations (10^{-14} – $2 \cdot 10^{-1}$ gL $^{-1}$). Dependences of I^{rel}_{Ox} and ROS^{rel}_{Ox} on concentration of Gd@Flu were compared.

It should be noted that initially we studied time-courses of ROS content in control samples (i.e., without Gd@Flu) of bacterial and enzymatic systems in model solutions for the time of bioluminescent experiment, 45 min. We found that the ROS content in the control enzyme solutions (enzymes + 1,4-benzoquinone at $EC_{50} = 10^{-5}$ M) and in the control bacterial suspensions (bacteria + 1,4-benzoquinone at $EC_{50} = 8 \cdot 10^{-7}$ M) were almost constant—about $4.5 \cdot 10^{-5}$ M and $5.8 \cdot 10^{-6}$ M, respectively.

Figure 3 presents values of I^{rel}_{Ox} and ROS^{rel}_{Ox} in solutions of organic oxidizer, 1,4-benzoquinone, in the bacterial and enzymatic systems (Figure 3A,B, respectively).

Figure 3A shows that Gd@Flu detoxifies the 1,4-benzoquinone solutions in bacterial suspension (curve 1) in the concentration ranges of 10^{-3} – $2 \cdot 10^{-1}$ gL $^{-1}$ ($I^{rel}_{Ox} > 1$, $p < 0.05$) with the maximal value of $I^{rel}_{Ox} = 1.75$.

Mitigation of the bacterial response to the oxidative load was observed not only in the solutions of organic oxidizer. In the solutions of inorganic oxidizer, potassium ferricyanide (curve 1, Figure S3, Supplementary Materials), Gd@Flu revealed moderate but reliable deviations of I^{rel}_{Ox} from the control ($p < 0.05$) with the maximal value of $I^{rel}_{Ox} = 1.2$ at a concentration range 10^{-7} – 10^{-2} gL $^{-1}$ ($p < 0.05$).

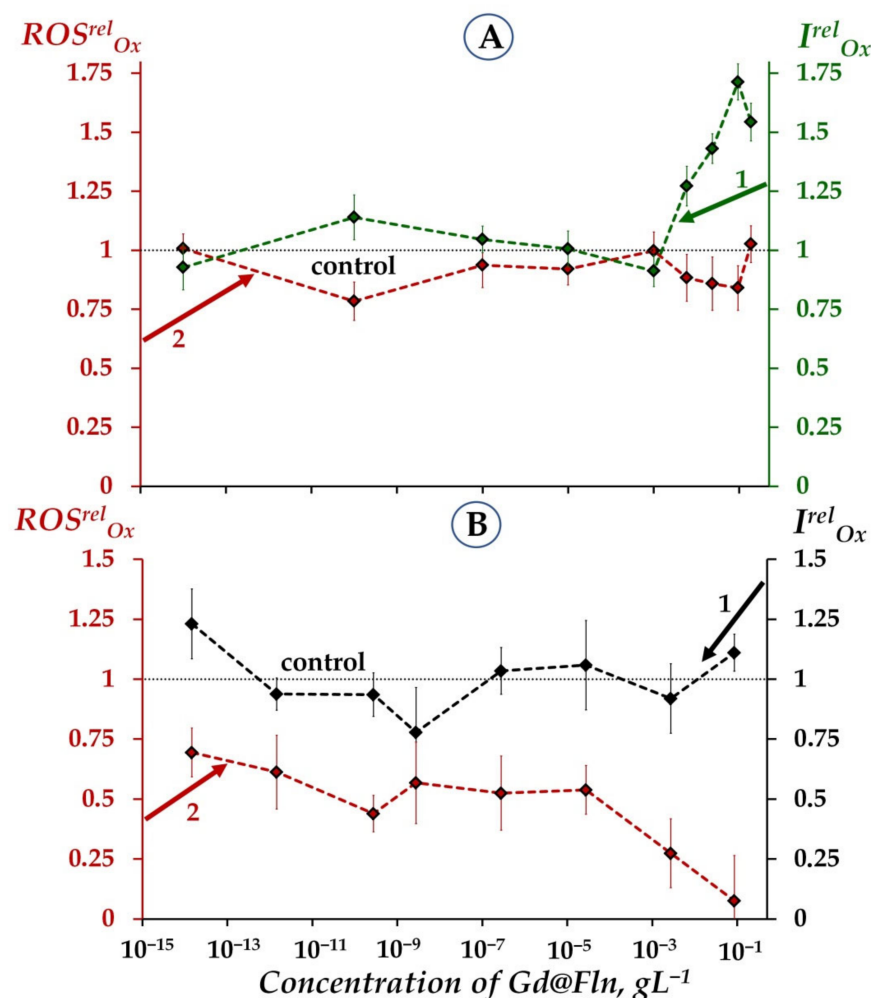


Figure 3. Antioxidant coefficients, I_{Ox}^{rel} , (1) and relative ROS content, ROS^{rel}_{Ox} , (2) in bacterial suspension (A) and enzymatic system (B) vs. concentration of fullerene Gd@Fln. Time of exposure to Gd@Fln was 45 min. Concentrations of ROS in the control bacterial suspension (bacteria + 1,4-benzoquinone at $EC_{50} = 8 \cdot 10^{-7}$ M) and control enzymatic system (enzymes + 1,4-benzoquinone at $EC_{50} = 10^{-5}$ M) were $5.8 \cdot 10^{-6}$ M and $4.9 \cdot 10^{-5}$ M, respectively. “Control” corresponds to the absence of Gd@Fln in the experimental solutions.

Similar behavior of other fullerenols was observed earlier [54–56,58,59]; higher antioxidant effects were observed in solutions of the organic oxidizer (1,4-benzoquinone). The difference in detoxifying ability of the fullerenols can be related to the hydrophobic/hydrophilic properties of the model oxidizers, and the involvement of hydrophobic fragments of the organic oxidizer in the detoxifying process in cellular or enzymatic systems. Hence, our results can be considered as an additional indirect confirmation of the importance of hydrophobic interactions in the bioeffects of Gd@Fln discussed in Section 2.1.1.

Figure 3A (curve 2) demonstrates that Gd@Fln did not noticeably change ROS content in bacterial suspension + 1,4-benzoquinone at all Gd@Fln concentrations used.

We analyzed correlations between concentration dependences of I_{Ox}^{rel} and ROS^{rel}_{Ox} in bacterial suspensions (Figure 3A) under conditions of oxidative exposure (i.e., in solutions of 1,4-benzoquinone) at a concentration range of Gd@Fln: 10^{-14} – $2 \cdot 10^{-1}$ gL⁻¹. This range revealed a moderate negative correlation ($r = -0.7$, $p < 0.05$, Figure 3A). This correlation demonstrates the inverse dependence between bacterial bioluminescence intensity and ROS content under conditions of oxidative stress, similar to the conditions without redox stress discussed previously (Section 2.1.3, Figure 2A). We can conclude that the mitigation of

model oxidative stress in bacterial suspension (i.e., bioluminescence activation) is concerned with the intensification of ROS consumption by the bacteria.

Notably, the maximal antioxidant coefficients of Gd@Flu, I_{Ox}^{rel} in the bacterial suspension rise with increased exposure time: from 1.4 (at 5-min exposure, Figure S4A, Supplementary Materials, curve 1) to 1.75 (45-min exposure, Figure 3A, curve 1), but ROS content does not change throughout the durations of the experiment.

Figure 3B reveals the absence of a noticeable antioxidant effect of Gd@Flu on the bioluminescence intensity of the enzyme system (curve 1): the value of I_{Ox}^{rel} was close to 1 in benzoquinone solution. Similarly, Gd@Flu did not affect the enzymatic bioluminescence ($I_{Ox}^{rel} \approx 1$) in solution of inorganic oxidizer, potassium ferricyanide (curve 2, Figure S3, Supplementary Materials).

The difference in responses of cellular and enzymatic systems to Gd@Flu in oxidizer solutions can be considered as an additional indirect confirmation of the importance of hydrophobic interactions and the involvement of cellular membrane in the bioeffects of Gd@Flu discussed in Section 2.1.1.

In contrast to the bacterial system (Figure 3A, curve 2), the enzymatic system demonstrated about 50% decrease in ROS content at a wide low-concentration range of Gd@Flu (10^{-14} – 10^{-4} gL⁻¹), Figure 3B, curve 2. We can suggest that Gd@Flu of low concentrations entirely neutralized the benzoquinone-induced excess of ROS in the enzyme solution. However, no reliable correlations between I_{Ox}^{rel} and ROS_{Ox}^{rel} were found in the enzymatic system. The result highlights the complexity of the processes responsible for the antioxidant effect of Gd@Flu.

2.2.2. Antioxidant Coefficients T_{Ox}^{rel} and ROS Content

Bioluminescent enzymatic system allows monitoring of not only bioluminescence intensity (I), but also of the bioluminescence induction period (T), Figure 6b, Section 3.2. The first parameter is used to study ‘general’ toxicity of foreign compounds, but the latter parameter is specific to oxidizers and responsible for ‘oxidative’ toxicity [54,98]. It is supposed that ‘oxidative’ toxicity is a function of redox activity of toxic media only, while ‘general’ toxicity is based on complex processes involving redox and polar/apolar interactions in the enzyme system [49].

In order to monitor changes in oxidative toxicity, the T-values were determined at different concentrations of Gd@Flu. The values of T_{Ox}^{rel} were calculated according to Equation (4) (Section 3.2).

Figure S5 (Supplementary Materials) demonstrates the dependences of T_{Ox}^{rel} on the concentration of fullerene Gd@Flu in solutions of 1,4-benzoquinone (curve 1) and $K_3[Fe(CN)_6]$ (curve 2). Antioxidant effects ($T_{Ox}^{rel} > 1$) were found in the solutions of both oxidizers; however, the average values of T_{Ox}^{rel} were low and did not exceed 1.1 in both cases.

Hence, we found that the antioxidant coefficients T_{Ox}^{rel} of Gd@Flu, calculated using induction bioluminescence period were lower than antioxidant coefficients I_{Ox}^{rel} , calculated using bioluminescence intensity. Similar observations were made in our previous studies of the other fullerenes [59]. This result provides more evidence of the importance of hydrophobic interactions in antioxidant activity of Gd@Flu.

2.2.3. Modeling of Oxidative Stress Conditions through ROS Content in Oxidizer Solutions

Modeling of conditions of oxidative stress is a subject of special interest; the content of ROS in solutions of model oxidizers in the presence and absence of biological molecules or living cells remains unexplored. The solution to this problem is important as it forms a basis for understanding the mechanism of ROS function in organisms and their environments. We try to elucidate this subject using aqueous media of different complexity: (1) solutions of oxidizers, (2) oxidizers + bacterial suspension, and (3) oxidizers + enzyme reactions.

Oxidizers of organic or inorganic types (1,4-benzoquinone or potassium ferricyanide $K_3[Fe(CN)_6]$, respectively) were used [70,98,99]. Standard redox potentials of these oxidiz-

ers are high: 0.71 V and 0.36 V, respectively [48–51,98]. Quinone and iron(III) are important representatives of intra-cellular and extra-cellular oxidizers. Additionally, quinones are shown to bind tightly to bacterial enzymes [70]. Quinones are produced environmentally as a result of the oxidative transformation of phenols and occupy the third position in the list of top widespread pollutants (after oil products and metal salts) [100]. Phenolic substances are also synthesized by soil bacteria as molecular signaling molecules in microbial communication and as adaptogens [101] and induce redox transformations in soils and aquifers, especially at low pH in the presence of iron(III) [102,103].

Figure 4 shows an increase in ROS content in benzoquinone solutions at concentrations $> 10^{-7}$ M for both cases—in iso-osmotic 3%NaCl solutions in the presence and absence of the bacteria ($ROS^{rel} > 1$, curves 1 and 2). It is seen that bacteria mitigate ROS increase at concentration $> 10^{-5}$ M; however, natural bacterial ROS production is effective at low concentrations of 1,4-benzoquinone (10^{-7} – 10^{-4} M) (compare curves 1 and 2 in Figure 4). Hence, the involvement of bacteria in ROS regulation in solutions of organic oxidizer is evident; bacteria increase (at low oxidizer concentrations) or decrease (at higher oxidizer concentrations) ROS content in oxidizer solutions.

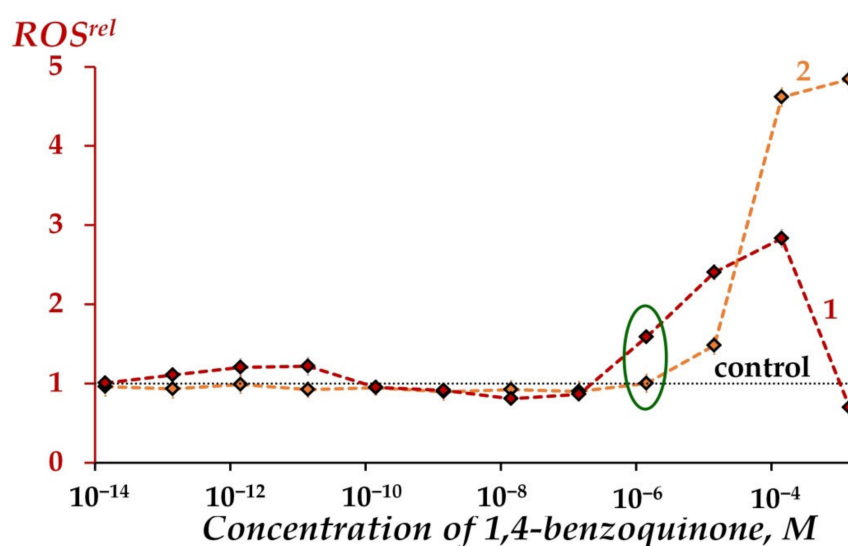


Figure 4. Relative ROS content, ROS^{rel} , in bacterial suspension (1), physiological 3%NaCl solution without bacteria (2) at different concentrations of 1,4-benzoquinone, 5 min exposure. Concentrations of ROS were $1.3 \cdot 10^{-5}$ M and $4.8 \cdot 10^{-6}$ M in the control physiological 3%NaCl solution and control bacterial suspension, respectively. Relative ROS content at EC_{50} marked with green ellipse. “Control” corresponds to the absence of 1,4-benzoquinone in the experimental solutions.

We found that 1,4-benzoquinone increased ROS content, $ROS^{rel} > 1$, in aqueous solutions at all concentrations studied, and in enzyme systems at $\leq 10^{-4}$ M, curves 1 and 2, Figure 5. This figure demonstrates the mitigation of ROS increase in enzymatic processes (as compared to aqueous solutions) in the entire range of 1,4-benzoquinone concentrations. This effect is a result of the consumption of ROS during the course of oxidative bioluminescence reactions of bacterial luciferase (reaction 2, Section 3.2) as discussed above (See Section 2.1.3).

The differences in effects of bacterial and enzyme reactions on ROS content in aqueous solutions might be concerned with the different level of organization of these two biological systems. This difference is a highly important and interesting subject; it should be clarified in detail during further investigations.

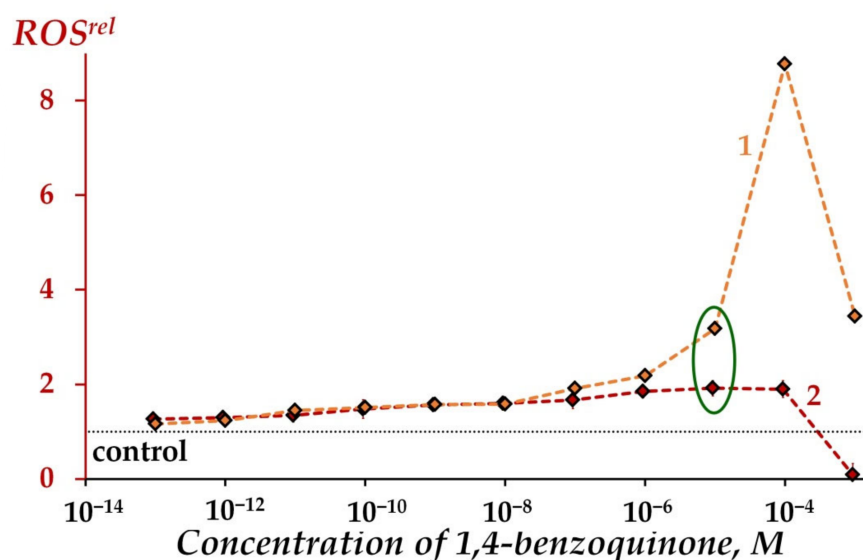


Figure 5. Relative ROS content, ROS^{rel} , in distilled water (1), enzymatic system (2) at different concentrations of 1,4-benzoquinone, 5 min exposure. Concentrations of ROS were $4.5 \cdot 10^{-7}$ M and $1.9 \cdot 10^{-5}$ M in distilled water and enzymatic system, respectively. “Control” corresponds to the absence of 1,4-benzoquinone in the experimental solutions.

3. Materials and Methods

3.1. Preparation of Fullereneol Gd@Fln

Gd-endohedral fullereneol $Gd@C_{82}O_y(OH)_x$, where $x + y = 40-42$ (Gd@Fln) was produced by fullerene $Gd@C_{82}$ hydroxylation in nitric acid followed by the hydrolysis of the polynitrofullerenes [104–107]. Mixture of fullerenes, involving $Gd@C_{82}$, was preliminarily synthesized by carbon helium high-frequency arc plasma at 98 kPa [107,108]. To determine Gd-content, fullerene mixtures were analyzed by atomic emission spectroscopy using calibration curve of the emission intensity versus Gd concentration [109]. The mass spectrum showed encapsulated Gd only ($Gd@C_{82}$). The $Gd@C_{82}$ -fullerene content in fullerene mixture was determined as 4.8%. The reaction of complexation with Lewis acids ($TiCl_4$) was used for enrichment of the extract of fullerene mixture by endohedral metallofullerenes ($Gd@C_{82}$) [110]. Then, $Gd@C_{82}$ was extracted with carbon disulfide from carbon soot.

The fullerene preparation was characterized with infrared spectroscopy in the KBr matrix using Fourier spectrometer VERTEX 70 (Bruker, Germany). The number of -OH groups was estimated by X-ray photoelectron spectroscopy (XPS) using UNI-SPECS spectrometer (SPECS GmbH, Germany) [111,112]. Both XPS and infrared (IR) spectra of endohedral Gd-containing fullereneol are presented in Figures S6 and S7 (Supplementary Materials).

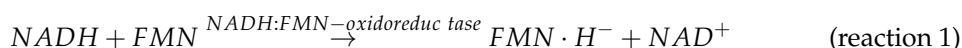
3.2. Bioluminescence Assay Systems and Experimental Data Processing

Antioxidant activity and toxicity of fullereneol Gd@Fln were evaluated using bioluminescence assay systems, cellular and enzymatic: (1) bacterial assay, i.e., intact marine luminous bacteria *Photobacterium phosphoreum*, strain 1883 IBSO from the Collection of Luminous Bacteria CCIBSO 863, Institute of Biophysics SB RAS, and (2) enzymatic assay, i.e., enzymatic preparation based on the system of coupled enzyme reactions catalyzed by NADH:FMN-oxidoreductase from *Vibrio fischeri* (0.15 a.u.) and luciferase from *Photobacterium leiognathi*, 0.5 mg/mL [113]. The enzyme preparation was produced at the Institute of Biophysics SB RAS (Krasnoyarsk, Russia). Antioxidant activity of Gd@Fln was assessed in model oxidizer solutions (in aqueous or 3% NaCl solutions of $K_3[Fe(CN)_6]$ for enzymatic and bacterial systems, respectively, and in 0.05 M phosphate buffer or 3% NaCl solutions of 1,4-benzoquinone for enzymatic and bacterial systems, respectively).

The chemicals were: FMN and tetradecanal from SERVA, Heidelberg, Germany; NADH from ICN Biochemicals, Costa-Mesa, CA, USA; sodium chloride (NaCl) from Khimreaktiv, Nizhny Novgorod, Russia; potassium ferricyanide ($K_3[Fe(CN)_6]$) and 1,4-benzoquinone from Sigma-Aldrich, St. Louis, MO, USA; potassium di-hydrogen phosphate (KH_2PO_4) and di-potassium hydrogen phosphate (K_2HPO_4) from Panreac, Barcelona, Spain. The reagents were of chemical or analytical grade.

To prepare the enzymatic assay system we used 0.1 mg/mL of enzyme preparation, $4 \cdot 10^{-4}$ M NADH, $5.4 \cdot 10^{-4}$ M FMN, and 0.0025% tetradecanal solutions. The NADH and tetradecanal were dissolved in 0.05 M phosphate buffer, pH 6.8, at 25 °C; FMN in distilled water. Concentration of NADH, FMN, and tetradecanal solutions in experimental samples were $1.6 \cdot 10^{-4}$ M, $5.4 \cdot 10^{-5}$ M, 0.0025%, respectively.

The enzymatic assay system is based on the following coupled enzymatic reactions:



For the cultivation of *P. phosphoreum* 1883 IBSO, the semisynthetic medium containing: 10 gL^{-1} tryptone, 28.5 gL^{-1} NaCl, 4.5 gL^{-1} $MgCl_2 \cdot 6H_2O$, 0.5 gL^{-1} $CaCl_2$, 0.5 gL^{-1} KCl, 3 gL^{-1} yeast extract, and 12.5 gL^{-1} agar was used. *P. phosphoreum* was plated on 25 mL of semisynthetic medium and incubated at 25 °C for a period of 24 h (stationary growth phase corresponding to maximum bioluminescence) in an incubator (WIS-20R, WiseCube Laboratory Instruments, Wertheim, Germany). Prior to experiments, bacteria were collected by pipetting of 3% NaCl solution directly onto the agar to release bacteria. The 3% NaCl solutions were used to imitate a marine environment for the bacterial cells and to balance osmotic processes. The bacterial suspension was diluted to $Abs_{660} = 0.025$ and stored at 4 °C for 30 min to allow bioluminescence stabilization. The reagents for bacterial cultivation were: tryptone and yeast extract from Dia-M, Moscow, Russia; sodium chloride (NaCl) from Khimreaktiv, Nizhny Novgorod, Russia; magnesium chloride hexahydrate ($MgCl_2 \cdot 6H_2O$), calcium chloride ($CaCl_2$), and potassium chloride (KCl) from Panreac AppliChem GmbH, Darmstadt, Germany; agar from Difco Laboratories, Detroit, MI, USA.

Toxic effects of Gd@Flu on bioluminescence of bacterial and enzymatic assay systems were characterized by relative bioluminescence intensity, I^{rel} :

$$I^{rel} = I_F/I_{contr} \quad (1)$$

where, I_{contr} and I_F are maximal bioluminescence intensities in the absence and presence of Gd@Flu, respectively.

The effective concentration of Gd@Flu inhibiting bioluminescence intensity by 50% ($I^{rel} = 0.5$), EC_{50} , were determined to evaluate its toxic effect.

It should be noted that we excluded an additional reason for the bioluminescence suppression—the effect of “optic filter” which is a result of bioluminescence absorption/reabsorption. All experiments with ‘colored’ solutions of Gd@Flu excluded effect of ‘optic filter’ (optical density of fullereneol solutions was <0.1 at the maximal bioluminescence light emittance wavelength—490 nm) [114], and this effect did not skew the results of the toxicological measurements.

To study antioxidant properties of Gd@Flu, we used conditions of a model oxidative stress for the bioluminescence assay systems using model oxidizers (Ox)—potassium ferricyanide ($K_3[Fe(CN)_6]$) and 1,4-benzoquinone; I_{contr} and I_{Ox} were measured as shown in Figure 6. Effective concentration EC_{50} of the model oxidizers inhibiting bioluminescence intensity by 50%, ($I^{rel}_{Ox} = 0.5$), EC_{50} , were determined with bacterial and enzymatic bioluminescence assays:

$$I^{rel}_{Ox} = I_{Ox}/I_{contr} \quad (2)$$

where, I_{contr} and I_{Ox} are maximal bioluminescence intensities in the absence and presence of model oxidizer, respectively, Figure 6.

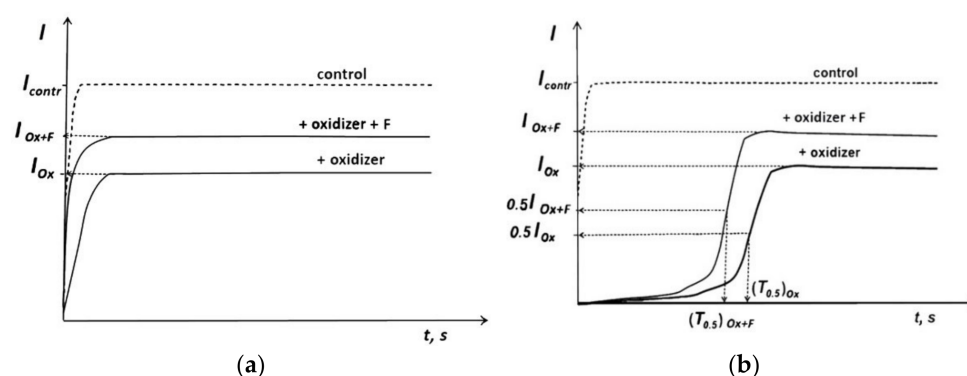


Figure 6. Bioluminescence kinetics in a solution of model oxidizer (Ox) and fullereneol (F): (a) cellular assay; (b) enzymatic assay.

The EC_{50} values of 1,4-benzoquinone were $8 \cdot 10^{-7}$ M and 10^{-5} M, EC_{50} values of $K_3[Fe(CN)_6]$ were 10^{-3} M and 10^{-6} M for bacterial and enzymatic assays, respectively. The values are close to those determined earlier [48,50]. The effect of “optic filter” was also excluded in these measurements.

Antioxidant activity of Gd@Fln was assessed under the conditions of the model oxidative stress. The values of EC_{50} of the oxidizers were used in these experiments to imitate oxidative stress conditions. A higher concentration range of Gd@Fln inhibiting the bioluminescence intensity was preliminarily determined and was not used in the experiments.

Both bioluminescent assays, bacterial and enzymatic, were applied to study changes in general toxicity in the oxidizer solutions under addition of Gd@Fln, the antioxidant coefficients I^{rel}_{Ox} were determined as follows:

$$I^{rel}_{Ox} = I_{Ox+F} / I_{Ox} \quad (3)$$

where I_{Ox} , I_{Ox+F} are bioluminescence intensities in oxidizer solutions at EC_{50} in the absence and presence of Gd@Fln, respectively, Figure 6.

The bioluminescence enzymatic assay was used to characterize changes in oxidative toxicity in the oxidizer solutions under the fullereneol exposure, the antioxidant coefficients T^{rel}_{Ox} were determined as follows:

$$T^{rel}_{Ox} = (T_{0.5})_{Ox} / (T_{0.5})_{Ox+F} \quad (4)$$

where $(T_{0.5})_{Ox}$ and $(T_{0.5})_{Ox+F}$ are bioluminescence induction periods in the oxidizer solutions in the absence and presence of Gd@Fln, respectively (Figure 6b).

Values of I^{rel}_{Ox} and T^{rel}_{Ox} were determined at different concentrations of Gd@Fln (10^{-14} – $2 \cdot 10^{-1}$ gL $^{-1}$). Values of $I^{rel}_{Ox} > 1$ or $T^{rel}_{Ox} > 1$ revealed a decrease in ‘general’ or ‘oxidative’ toxicities, respectively, under the exposure to Gd@Fln, i.e., antioxidant activity of Gd@Fln in solutions of oxidizers. Values of $I^{rel}_{Ox} \approx 1$ or $T^{rel}_{Ox} \approx 1$ revealed the absence of the Gd@Fln effects.

All bioluminescence measurements were conducted in five replicates for all solutions. Bioluminescence intensities of bacterial and enzymatic assays were measured without pre-incubation.

3.3. Luminol Chemiluminescence Assay

We used luminol chemiluminescence method to evaluate the content of Reactive Oxygen Species (ROS) in the experimental bacterial suspensions and enzymatic solutions [115,116]. This technique is used to determine an integral content of ROS assuming that a dynamic equilibrium of the different ROS forms takes place.

Reagents for the chemiluminescence measurements were: luminol ($C_8H_7N_3O_2$) and potassium ferricyanide ($K_3[Fe(CN)_6]$) from Sigma-Aldrich (St. Louis, MO, USA), 3%

solution of H₂O₂ from Tula Pharmaceutical Factory (Tula, Russia), potassium hydroxide (KOH) from Khimreactiv (Nizhny Novgorod, Russia). All reagents were of chemical grade.

Stock luminol solution (10⁻² M) was prepared as follows: luminol powder was dissolved in 5 mL in 1M solution of KOH and then 5 mL of distilled water was added. The chemiluminescence luminol reaction was initiated by K₃[Fe(CN)₆]; maximal value of chemiluminescence intensity was determined. Concentrations of luminol and K₃[Fe(CN)₆] in the experimental samples were 2·10⁻⁵ M and 3·10⁻⁴ M, respectively. The chemiluminescence registration was carried out immediately following the bioluminescence measurements in the same bacterial and enzymatic samples.

All chemiluminescence measurements were carried out in five replicates.

Initially, the dependences of chemiluminescence intensity on concentration of H₂O₂ were determined in distilled water and 3% NaCl solution for enzymatic and bacterial luminescence systems, respectively; they were used as calibration dependences to evaluate ROS content in all experimental samples.

Chemiluminescence intensities were measured in bioluminescence assay systems (bacterial and enzymatic), as well as in bacteria-free/enzyme-free aqueous solutions. Time-courses of I^{rel} and ROS^{rel} were obtained at different concentrations of 1,4-benzoquinone (10⁻¹³–10⁻³ M), Gd@Flu (10⁻¹⁸–3 gL⁻¹), and combinations of 1,4-benzoquinone (at EC₅₀) and Gd@Flu (10⁻¹⁸–3 gL⁻¹). Optical density of fullereneol or 1,4-benzoquinone solutions was <0.1 at the maximum of the chemiluminescence light emittance ($Abs_{425} < 0.1$); hence, the effect of “optic filter” was excluded (See Section 3.2).

The relative values of ROS content (ROS^{rel}) were calculated as ratios of ROS content in the experimental solutions to that in the control solutions.

3.4. Equipment

Bioluminescence and chemiluminescence intensity were measured with biochemiluminometer Luminoskan Ascent (Thermo Electron Corporation, Solon, OH, USA) equipped with injector system. All luminescence measurements were carried out at 25 °C. Optical density, D , of the fullereneol or 1,4-benzoquinone solutions and bacterial suspensions were measured using a double-beam spectrophotometer UVIKON-943 (KONTRON Instruments, Milano, Italy).

3.5. Statistical Processing

The SD-values for I^{rel} , I^{rel}_{Ox} , T^{rel}_{Ox} or ROS^{rel} were calculated using GraphPad Prism 8 (GraphPad Software, San Diego, CA, USA). They did not exceed 15%, 17%, 13% and 20%, respectively.

To reveal correlations between the bioluminescence signal and ROS concentrations, a statistical dependence between rankings of two variables was analyzed [117], correlation coefficients r were calculated.

Statistical processing of the results of bioluminescence and chemiluminescence assays was carried out; p -values were calculated with GraphPad Prism 8 using ANOVA. The p -values were assessed by Kruskal–Wallis test of two independent sample distributions.

4. Conclusions

Our current paper considers the biological activity (toxicity and antioxidant activity) of endohedral gadolinium fullereneol (Gd@Flu) which involved 82 carbon atoms and 40–42 oxygen groups on the surface of the carbon cage. We found that Gd@Flu inhibited bacterial and enzymatic bioluminescence at high concentrations >2·10⁻¹ gL⁻¹, producing a minimal toxic effect among the previously studied fullereneols. The Gd@Flu moderately activates bacterial cells under lower-concentration exposures: 10⁻³ gL⁻¹–2·10⁻¹ gL⁻¹. The activation processes were accompanied by a consumption of reactive oxygen species (ROS); the bacteria effectively mitigated an increase in ROS content induced by Gd@Flu in aqueous solutions. The results contribute to understanding the molecular mechanism of “hormetic” responses of cells to exposure to low concentrations of bioactive compounds.

The antioxidant activity of Gd@Fln was found at its low and ultralow concentrations ($<2 \cdot 10^{-1} \text{ gL}^{-1}$) under the conditions of model oxidative stress, antioxidant coefficients I^{rel}_{Ox} were higher in organic oxidizer solutions than in inorganic ones; this highlights the importance of hydrophobic interactions in redox transformations.

Reactive oxygen species (ROS) were considered as active particles responsible for inhibiting (toxic) and activating effects in the bioassays. We found that both effects are concerned with a decrease in ROS content under the addition of the fulleranol.

We should emphasize that not only excess of ROS can produce a deleterious effect on biological systems, as conventionally stated in biomedical literature, but the lack of ROS can suppress biological functions as well, as is shown in our current investigation.

Hence, our study demonstrated a suitability and high potential for the bioluminescence-based biosensing procedure for the detailed study of the biological activity of carbon nanoparticles with Gd@Fln as an example.

In the frames of our nearest prospective studies, we plan to investigate biological activity of another homologous endohedral fulleranol with lower number of oxygen substituents—Gd@C₈₂O_y(OH)_x, where $x + y = 20\text{--}24$. We plan to determine its toxic and antioxidant characteristics through similar methods, compare them with those of the Gd@Fln studied in this work, and evaluate its biomedical applicability. According to current theoretical speculations [61], fulleranol with lower number of oxygen substituents should display higher electron affinity, which ensures advanced antioxidant properties.

Supplementary Materials: The following supporting information can be downloaded at: <https://www.mdpi.com/article/10.3390/ijms23095152/s1>.

Author Contributions: Planning an experiment, experimental studies using bioluminescence and chemiluminescence methods, data processing, interpretation, data analysis, writing and editing the manuscript, E.S.S.; provision of fulleranol synthesis, qualitative and quantitative analysis of fulleranol, N.G.V.; provision of fullerene synthesis, G.N.C.; conceptualization, general leadership of the work, data analysis, writing—original draft preparation, writing—review and editing the manuscript, N.S.K. All authors have read and agreed to the published version of the manuscript.

Funding: This research was funded by Russian Foundation for Basic Research, N18-29-19003; Russian Foundation for Basic Research, Krasnoyarsk Territory and Krasnoyarsk Regional Fund of Science, N20-44-243001; and partly supported by the Program of the Federal Service for Surveillance on Consumer Rights Protection and Human Wellbeing, Fundamental Study 2020–2025 (Russia).

Acknowledgments: Authors thank M. Yehia for improvement of the manuscript style.

Conflicts of Interest: The authors declare no conflict of interest. The funders had no role in the design of the study; in the collection, analyses, or interpretation of data; in the writing of the manuscript, or in the decision to publish the results.

Abbreviations

EC ₅₀	effective concentration of oxidizers or fullerenols which inhibited bioluminescence intensity by 50%
F	fulleranol
FMN	flavinmononucleotide
Gd@Fln	Gd@C ₈₂ O _y (OH) _x , where $x + y = 40\text{--}42$
I	bioluminescence intensity
IR	infrared
MRI	magnetic resonance imaging
NADH	nicotinamide adenine dinucleotide, disodium salt, reduced
Ox	model oxidizer
ROS	reactive oxygen species
T	bioluminescence induction period
XPS	X-ray photoelectron spectroscopy

References

1. Foley, S.; Crowley, C.; Smaih, M.; Bonfils, C.; Erlanger, B.F.; Seta, P.; Larroque, C. Cellular localization of a water-soluble fullerene derivative. *Biochem. Biophys. Res. Commun.* **2002**, *294*, 116–119. [[CrossRef](#)]
2. Grebowski, J.; Krokosz, A.; Puchala, M. Fullereneol C₆₀(OH)₃₆ could associate to band 3 protein of human erythrocyte membranes. *Biochim. Biophys. Acta (BBA) Biomembr.* **2013**, *1828*, 2007–2014. [[CrossRef](#)]
3. Zheng, Y.; Hou, L.; Liu, M.; Newell, S.E.; Yin, G.; Yu, C.; Zhang, H.; Li, X.; Gao, D.; Gao, J.; et al. Effects of silver nanoparticles on nitrification and associated nitrous oxide production in aquatic environments. *Sci. Adv.* **2017**, *3*, e1603229. [[CrossRef](#)]
4. Bosi, S.; Ros, T.D.; Spalluto, G.; Prato, M. Fullerene derivatives: An attractive tool for biological applications. *Eur. J. Med. Chem.* **2003**, *38*, 913–923. [[CrossRef](#)]
5. Satoh, M.; Takayanagi, I. Pharmacological studies on fullerene (C₆₀), a novel carbon allotrope, and its derivatives. *J. Pharmacol. Sci.* **2006**, *100*, 513–518. [[CrossRef](#)]
6. Markovic, Z.; Trajkovic, V. Biomedical potential of the reactive oxygen species generation and quenching by fullerenes (C₆₀). *Biomaterials* **2008**, *29*, 3561–3573. [[CrossRef](#)]
7. Rondags, A.; Yuen, W.Y.; Jonkman, M.F.; Horvath, B. Fullerene C₆₀ with cytoprotective and cytotoxic potential: Prospects as a novel treatment agent in Dermatology? *Exp. Dermatol.* **2016**, *26*, 220–224. [[CrossRef](#)]
8. Zhao, Y.; Shen, X.; Ma, R.; Hou, Y.; Qian, Y.; Fan, C. Biological and biocompatible characteristics of fullerene nanomaterials for tissue engineering. *Histol. Histopathol.* **2021**, *36*, 725–731. [[CrossRef](#)]
9. Sharoyko, V.V.; Ageev, S.V.; Podolsky, N.E.; Petrov, A.V.; Litasov, E.V.; Vlasov, T.D.; Vasina, L.V.; Murin, I.V.; Piotrovskiy, L.B.; Semenov, K.N. Biologically active water-soluble fullerene adducts: Das Glasperlenspiel (by H. Hesse)? *J. Mol. Liq.* **2021**, *323*, 114990. [[CrossRef](#)]
10. Jovic, D.; Jacevic, V.; Kuca, K.; Borišev, I.; Mrdjanovic, J.; Petrovic, D.; Seke, M.; Djordjevic, A. The puzzling potential of carbon nanomaterials: General properties, application, and toxicity. *Nanomaterials* **2020**, *10*, 1508. [[CrossRef](#)]
11. McEwen, C.N.; McKay, R.G.; Larsen, B.S. C₆₀ as a radical sponge. *J. Am. Chem. Soc.* **1992**, *114*, 4412–4414. [[CrossRef](#)]
12. Grebowski, J.; Kazmierska, P.; Krokosz, A. Fullerenols as a new therapeutic approach in nanomedicine. *Biomed. Res. Int.* **2013**, *2013*, 751913. [[CrossRef](#)] [[PubMed](#)]
13. Cai, X.; Hao, J.; Zhang, X.; Yu, B.; Ren, J.; Luo, C.; Li, Q.; Huang, Q.; Shi, X.; Li, W.; et al. The polyhydroxylated fullerene derivative C₆₀(OH)₂₄ protects mice from ionizing-radiation-induced immune and mitochondrial dysfunction. *Toxicol. Appl. Pharmacol.* **2010**, *243*, 27–34. [[CrossRef](#)]
14. Slavic, M.; Djordjevic, A.; Radojicic, R.; Milovanovic, S.; Orescanin-Dusic, Z.; Rakocevic, Z.; Spasic, M.B.; Blagojevic, D. Fullereneol C₆₀(OH)₂₄ nanoparticles decrease relaxing effects of dimethyl sulfoxide on rat uterus spontaneous contraction. *J. Nanopart. Res.* **2013**, *15*, 1650. [[CrossRef](#)]
15. Mirkov, S.M.; Djordjevic, A.N.; Andric, N.L.; Andric, S.A.; Kostic, T.S.; Bogdanovic, G.M.; Vojinovic-Miloradov, M.B.; Kovacevic, R.Z. Nitric oxide-scavenging activity of polyhydroxylated fullereneol, C₆₀(OH)₂₄. *Nitric Oxide* **2004**, *11*, 201–207. [[CrossRef](#)] [[PubMed](#)]
16. Injac, R.; Prijatelj, M.; Strukelj, B. Fullereneol nanoparticles: Toxicity and antioxidant activity. *Methods Mol. Biol.* **2013**, *1028*, 75–100. [[CrossRef](#)]
17. Djordjevic, A.; Srdjenovic, B.; Seke, M.; Petrovic, D.; Injac, R.; Mrdjanovic, J. Review of synthesis and antioxidant potential of fullereneol nanoparticles. *J. Nanomater.* **2015**, *2015*, 567073. [[CrossRef](#)]
18. Wang, Z.; Wang, S.; Lu, Z.; Gao, X. Syntheses, structures and antioxidant activities of fullereneols: Knowledge learned at the atomistic level. *J. Clust. Sci.* **2015**, *26*, 375–388. [[CrossRef](#)]
19. Djordjevic, A.; Canadanovic-Brunet, J.M.; Vojinovic-Miloradov, M.; Bogdanovic, G. Antioxidant properties and hypothetical radical mechanism of fullereneol C₆₀(OH)₂₄. *Oxid. Commun.* **2005**, *27*, 806–812.
20. Jiao, F.; Liu, Y.; Qu, Y.; Li, W.; Zhou, G.; Ge, C.; Li, Y.; Sun, B.; Chen, C. Studies on anti-tumor and antimetastatic activities of fullereneol in a mouse breast cancer model. *Carbon* **2010**, *48*, 2231–2243. [[CrossRef](#)]
21. Meng, J.; Liang, X.; Chen, X.; Zhao, Y. Biological characterizations of [Gd@C₈₂(OH)₂₂]_n nanoparticles as fullerene derivatives for cancer therapy. *Integr. Biol.* **2013**, *5*, 43–47. [[CrossRef](#)]
22. Cui, X.; Xu, S.; Wang, X.; Chen, C. The nano-bio interaction and biomedical applications of carbon nanomaterials. *Carbon* **2018**, *138*, 436–450. [[CrossRef](#)]
23. Maravilla, K.R.; San-Juan, D.; Kim, S.J.; Elizondo-Riojas, G.; Fink, J.R.; Escobar, W.; Bag, A.; Roberts, D.R.; Hao, J.; Pitrou, C.; et al. Comparison of Gadoterate Meglumine and Gadobutrol in the MRI Diagnosis of Primary Brain Tumors: A Double-Blind Randomized Controlled Intraindividual Crossover Study (the REMIND Study). *AJNR Am. J. Neuroradiol.* **2017**, *38*, 1681–1688. [[CrossRef](#)]
24. Ersoy, H.; Rybicki, F.J. Biochemical Safety Profiles of Gadolinium-Based Extracellular Contrast Agents and Nephrogenic Systemic Fibrosis. *J. Magn. Reson. Imaging* **2007**, *26*, 1190–1197. [[CrossRef](#)]
25. Clavaguera, C.; Sansot, E.; Calvo, F.; Dognon, J.P. Gd(III) polyaminocarboxylate chelate: Realistic many-body molecular dynamics simulations for molecular imaging applications. *J. Phys. Chem.* **2006**, *110*, 12848–12851. [[CrossRef](#)]
26. Sosnovik, D.E.; Caravan, P. Molecular MRI of the Cardiovascular System in the Post-NSF Era. *Curr. Cardiovasc. Imaging Rep.* **2013**, *6*, 61–68. [[CrossRef](#)]

27. Kanda, T.; Osawa, M.; Oba, H.; Toyoda, K.; Kotoku, J.; Haruyama, T.; Takeshita, K.; Furui, S. High signal intensity in dentate nucleus on unenhanced T1-weighted MR Images: Association with linear versus macrocyclic gadolinium chelate administration. *Radiology* **2015**, *275*, 803–809. [[CrossRef](#)]
28. Ooi, L.P.; Crawford, D.H.; Gotley, D.C.; Clouston, A.D.; Strong, R.W.; Gobe, G.C.; Halliday, J.W.; Bridle, K.R.; Ramm, G.A. Evidence that “myofibroblast-like” cells are the cellular source of capsular collagen in hepatocellular carcinoma. *J. Hepatol.* **1997**, *26*, 798–807. [[CrossRef](#)]
29. Liang, X.-J.; Meng, H.; Wang, Y.; He, H.; Meng, J.; Lu, J.; Wang, P.C.; Zhao, Y.; Gao, X.; Sun, B.; et al. Metallofullerene nanoparticles circumvent tumor resistance to cisplatin by reactivating endocytosis. *Proc. Natl. Acad. Sci. USA* **2010**, *107*, 7449–7454. [[CrossRef](#)]
30. Popov, A.A.; Yang, S.; Dunsch, L. Endohedral Fullerenes. *Chem. Rev.* **2013**, *113*, 5989–6113. [[CrossRef](#)]
31. Shinohara, H. Endohedral metallofullerenes. *Rep. Prog. Phys.* **2000**, *63*, 843–892. [[CrossRef](#)]
32. Yang, S.; Wei, T.; Jin, F. When metal clusters meet carbon cages: Endohedral clusterfullerenes. *Chem. Soc. Rev.* **2017**, *46*, 5005–5058. [[CrossRef](#)] [[PubMed](#)]
33. Wang, Z.; Gao, X.; Zhao, Y. Mechanisms of Antioxidant Activities of Fullerlenols from First-Principles Calculation. *J. Phys. Chem.* **2018**, *122*, 8183–8190. [[CrossRef](#)] [[PubMed](#)]
34. Zhang, J.; Ye, Y.; Chen, Y.; Pregot, C.; Li, T.; Balasubramaniam, S.; Hobart, D.B.; Zhang, Y.; Wi, S.; Davis, R.M.; et al. Gd₃N@C₈₄(OH)_x: A New Egg-Shaped Metallofullerene Magnetic Resonance Imaging Contrast Agent. *J. Am. Chem. Soc.* **2014**, *136*, 2630–2636. [[CrossRef](#)] [[PubMed](#)]
35. Chen, C.; Xing, G.; Wang, J.; Zhao, Y.; Li, B.; Tang, J.; Jia, G.; Wang, T.; Sun, J.; Xing, L.; et al. Multihydroxylated [Gd@C₈₂(OH)₂₂]_n Nanoparticles: Antineoplastic Activity of High Efficiency and Low Toxicity. *Nano Lett.* **2005**, *5*, 2050–2057. [[CrossRef](#)]
36. Kang, S.G.; Huynh, T.; Zhou, R. Non-destructive Inhibition of Metallofullerenol Gd@C₈₂(OH)₂₂ on WW domain: Implication on Signal Transduction Pathway. *Sci. Rep.* **2012**, *2*, 957. [[CrossRef](#)] [[PubMed](#)]
37. Kang, S.G.; Zhou, G.; Yang, P.; Liu, Y.; Sun, B.; Huynh, T.; Meng, H.; Zhao, L.; Xing, G.; Chen, C.; et al. Molecular mechanism of pancreatic tumor metastasis inhibition by Gd@C₈₂(OH)₂₂ and its implication for de novo design of nanomedicine. *Proc. Natl. Acad. Sci. USA* **2012**, *109*, 15431–15436. [[CrossRef](#)]
38. Li, J.; Cui, R.; Chang, Y.; Guo, X.; Gu, W.; Huang, H.; Chen, K.; Lin, G.; Dong, J.; Xing, G.; et al. Adaption of the structure of carbon nanohybrids toward high-relaxivity for a new MRI contrast agent. *RSC Adv.* **2016**, *6*, 58028–58033. [[CrossRef](#)]
39. Tang, J.; Zhang, R.; Guo, M.; Zhou, H.; Zhao, Y.; Liu, Y.; Wu, Y.; Chen, C. Gd-metallofullerenol drug delivery system mediated macrophage polarization enhances the efficiency of chemotherapy. *J. Control. Release* **2020**, *320*, 293–303. [[CrossRef](#)]
40. Bulich, A.A.; Isenberg, D.L. Use of the luminescent bacterial system for rapid assessment of aquatic toxicity. *ISA Trans.* **1981**, *20*, 29–33.
41. Girotti, S.; Ferri, E.N.; Fumo, M.G.; Maiolini, E. Monitoring of environmental pollutants by bioluminescent bacteria. *Anal. Chim. Acta* **2008**, *608*, 2–29. [[CrossRef](#)] [[PubMed](#)]
42. Roda, A.; Pasini, P.; Mirasoni, M.; Michchelini, E.; Guardigli, M. Biotechnological application of bioluminescence and chemiluminescence. *Trends Biotechnol.* **2004**, *22*, 295–303. [[CrossRef](#)]
43. Abbas, M.; Adil, M.; Ehtisham-Ul-Haque, S.; Munir, B.; Yameen, M.; Ghaffar, A.; Shar, G.A.; Tahir, M.A.; Iqbal, M. *Vibrio fischeri* bioluminescence inhibition assay for ecotoxicity assessment: A review. *Sci. Total Environ.* **2018**, *626*, 1295–1309. [[CrossRef](#)] [[PubMed](#)]
44. Ismailov, A.D.; Aleskerova, L.E. Photobiosensors containing luminescent bacteria. *Biochemistry* **2015**, *80*, 733–744. [[CrossRef](#)] [[PubMed](#)]
45. Esimbekova, E.N.; Torgashina, I.G.; Kalyabina, V.P. Enzymatic Biotesting: Scientific Basis and Application. *Contemp. Probl. Ecol.* **2021**, *14*, 290–304. [[CrossRef](#)]
46. Esimbekova, E.N.; Kalyabina, V.P.; Kopylova, K.V.; Torgashina, I.G.; Kratasyuk, V.A. Design of bioluminescent biosensors for assessing contamination of complex matrices. *Talanta* **2021**, *233*, 122509. [[CrossRef](#)] [[PubMed](#)]
47. Kudryasheva, N.S. Bioluminescence and exogenous compounds: Physico-chemical basis for bioluminescent assay. *J. Photochem. Photobiol. B* **2006**, *83*, 77–86. [[CrossRef](#)]
48. Tarasova, A.S.; Stom, D.I.; Kudryasheva, N.S. Effect of humic substances on toxicity of inorganic oxidizer bioluminescent monitoring. *Environ. Toxicol. Chem.* **2011**, *30*, 1013–1017. [[CrossRef](#)]
49. Kudryasheva, N.S.; Tarasova, A.S. Pollutant toxicity and detoxification by humic substances: Mechanisms and quantitative assessment via luminescent biomonitoring. *Environ. Sci. Pollut. Res.* **2015**, *22*, 155–167. [[CrossRef](#)]
50. Tarasova, A.S.; Kislán, S.L.; Fedorova, E.S.; Kuznetsov, A.M.; Mogilnaya, O.A.; Stom, D.I.; Kudryasheva, N.S. Bioluminescence as a tool for studying detoxification processes in metal salt solutions involving humic substances. *J. Photochem. Photobiol. B* **2012**, *117*, 164–170. [[CrossRef](#)]
51. Tarasova, A.S.; Stom, D.I.; Kudryasheva, N.S. Antioxidant activity of humic substances via bioluminescent monitoring in vitro. *Environ. Monit. Assess.* **2015**, *187*, 89. [[CrossRef](#)] [[PubMed](#)]
52. Yehia, M.R.; Smolyarova, T.E.; Shabanov, A.V.; Sushko, E.S.; Badun, G.A.; Kudryasheva, N.S. Adaptation of a Bacterial Bioluminescent Assay to Monitor Bioeffects of Gold Nanoparticles. *Bioengineering* **2022**, *9*, 61. [[CrossRef](#)] [[PubMed](#)]
53. Kovel, E.S.; Sachkova, A.S.; Vnukova, N.G.; Churilov, G.N.; Knyazeva, E.M.; Kudryasheva, N.S. Antioxidant activity and toxicity of fullerlenols via bioluminescence signaling: Role of oxygen substituents. *Int. J. Mol. Sci.* **2019**, *20*, 2324. [[CrossRef](#)] [[PubMed](#)]

54. Kudryasheva, N.S.; Kovel, E.S.; Sachkova, A.S.; Vorobeva, A.A.; Isakova, V.G.; Churilov, G.N. Bioluminescent enzymatic assay as a tool for studying antioxidant activity and toxicity of bioactive compounds. *Photochem. Photobiol.* **2017**, *93*, 536–540. [[CrossRef](#)] [[PubMed](#)]
55. Sachkova, A.S.; Kovel, E.S.; Churilov, G.N.; Guseynov, O.A.; Bondar, A.A.; Dubinina, I.A.; Kudryasheva, N.S. On mechanism of antioxidant effect of fullerenols. *Biochem. Biophys. Rep.* **2017**, *9*, 1–8. [[CrossRef](#)]
56. Sachkova, A.S.; Kovel, E.S.; Churilov, G.N.; Stom, D.I.; Kudryasheva, N.S. Biological activity of carbonic nano-structures—comparison via enzymatic bioassay. *J. Soils Sediments* **2019**, *19*, 2689–2696. [[CrossRef](#)]
57. Kudryasheva, N.S.; Kovel, E.S. Monitoring of low-intensity exposures via luminescent bioassays of different complexity: Cells, enzyme reactions and fluorescent proteins. *Int. J. Mol. Sci.* **2019**, *20*, 4451. [[CrossRef](#)]
58. Sachkova, A.S.; Kovel, E.S.; Vorobeva, A.A.; Kudryasheva, N.S. Antioxidant activity of fullerenols. Bioluminescent monitoring in vitro. *Procedia Technol.* **2017**, *27*, 230–231. [[CrossRef](#)]
59. Kovel, E.S.; Kicheeva, A.G.; Vnukova, N.G.; Churilov, G.N.; Stepin, E.A.; Kudryasheva, N.S. Toxicity and Antioxidant Activity of Fullerene C₆₀ with Low Number of Oxygen Substituents. *Int. J. Mol. Sci.* **2021**, *22*, 6382. [[CrossRef](#)]
60. Bondarenko, L.S.; Kovel, E.S.; Kydraliev, K.A.; Dzhardimalieva, G.I.; Illé, E.; Tombácz, E.; Kicheeva, A.G.; Kudryasheva, N.S. Effects of Modified Magnetite Nanoparticles on Bacterial Cells and Enzyme Reactions. *Nanomaterials* **2020**, *10*, 1499. [[CrossRef](#)]
61. Shakirova, A.A.; Tomilin, F.N.; Pomogaev, V.A.; Vnukova, N.G.; Churilov, G.N.; Kudryasheva, N.S.; Tchaikovskaya, O.N.; Ovchinnikov, S.G.; Avramov, P.V. Synthesis, Mass Spectroscopy Detection, and Density Functional Theory Investigations of the Gd Endohedral Complexes of C₈₂ Fullerenes. *Computation* **2021**, *9*, 58. [[CrossRef](#)]
62. Zakharova, A.V.; Bedrina, M.E. A quantum chemical study of endometallofullerenes: Gd@C₇₀, Gd@C₈₂, Gd@C₈₄, and Gd@C₉₀. *Eur. Phys. J. D* **2020**, *74*, 116. [[CrossRef](#)]
63. Compagnon, I.; Antoine, R.; Broyer, M.; Dugourd, P.; Lermé, J.; Rayane, D. Electric polarizability of isolated C₇₀ molecules. *Phys. Rev. A* **2001**, *64*, 25201. [[CrossRef](#)]
64. Boltalina, O.; Ioffe, I.; Sorokin, I.; Sidorov, L.N. Electron Affinity of Some Endohedral Lanthanide Fullerenes. *J. Phys. Chem. A* **1997**, *101*, 9561–9563. [[CrossRef](#)]
65. Guha, S.; Nakamoto, K. Electronic structures and spectral properties of endohedral fullerenes. *Coord. Chem. Rev.* **2005**, *249*, 1111–1132. [[CrossRef](#)]
66. Kolesnik, O.V.; Rozhko, T.V.; Lapina, M.A.; Solovyev, V.S.; Sachkova, A.S.; Kudryasheva, N.S. Development of Cellular and Enzymatic Bioluminescent Assay Systems to Study Low-Dose Effects of Thorium. *Bioengineering* **2021**, *8*, 194. [[CrossRef](#)]
67. Rozhko, T.V.; Kolesnik, O.V.; Badun, G.A.; Stom, D.I.; Kudryasheva, N.S. Humic Substances Mitigate the Impact of Tritium on Luminous Marine Bacteria. Involvement of Reactive Oxygen Species. *Int. J. Mol. Sci.* **2020**, *21*, 6783. [[CrossRef](#)]
68. Rozhko, T.; Nogovitsyna, E.; Badun, G.; Lukyanchuk, A.; Kudryasheva, N. Reactive Oxygen Species and Low-Dose Effects of Tritium on Bacterial Cells. *J. Environ. Radioact.* **2019**, *208–209*, 106035. [[CrossRef](#)]
69. Kamnev, A.A.; Tugarova, A.V.; Selivanova, M.A.; Tarantilis, P.A.; Polissiou, M.G.; Kudryasheva, N.S. Effects of americium-241 and humic substances on *Photobacterium phosphoreum*: Bioluminescence and diffuse reflectance FTIR spectroscopic studies. *Spectrochim. Acta Part A Mol. Biomol. Spectrosc.* **2013**, *100*, 171–175. [[CrossRef](#)]
70. Vetrova, E.V.; Kudryasheva, N.S.; Cheng, K.H. Effect of quinone on the fluorescence decay dynamics of endogenous flavin bound to bacterial luciferase. *Biophys. Chem.* **2009**, *141*, 59–65. [[CrossRef](#)]
71. Balogh, L.P. Caging cancer. *Nanomedicine* **2015**, *11*, 867–869. [[CrossRef](#)] [[PubMed](#)]
72. Liu, J.; Kang, S.-G.; Wang, P.; Wang, Y.; Lv, X.; Liu, Y.; Wang, F.; Gu, Z.; Yang, Z.; Weber, J.K.; et al. Molecular mechanism of Gd@C₈₂(OH)₂₂ increasing collagen expression: Implication for engaging tumor. *Biomaterials* **2018**, *152*, 24–36. [[CrossRef](#)] [[PubMed](#)]
73. Liu, Y.; Chen, C.; Qian, P.; Lu, X.; Sun, B.; Zhang, X.; Wang, L.; Gao, X.; Li, H.; Chen, Z.; et al. Gd-metallofullerenol nanomaterial as non-toxic breast cancer stem cell-specific inhibitor. *Nat. Commun.* **2015**, *6*, 5988. [[CrossRef](#)]
74. Calabrese, E. Hormesis: Path and Progression to Significance. *Int. J. Mol. Sci.* **2018**, *19*, 2871. [[CrossRef](#)] [[PubMed](#)]
75. Jargin, S.V. Hormesis and Radiation Safety Norms: Comments for an Update. *Hum. Exp. Toxicol.* **2018**, *37*, 1233–1243. [[CrossRef](#)]
76. Shibamoto, Y.; Nakamura, H. Overview of Biological, Epidemiological, and Clinical Evidence of Radiation Hormesis. *Int. J. Mol. Sci.* **2018**, *19*, 2387. [[CrossRef](#)]
77. Ge, H.; Zhou, M.; Lv, D.; Wang, M.; Xie, D.; Yang, X.; Dong, C.; Li, S.; Lin, P. Novel Segmented Concentration Addition Method to Predict Mixture Hormesis of Chlortetracycline Hydrochloride and Oxytetracycline Hydrochloride to *Aliivibrio fischeri*. *Int. J. Mol. Sci.* **2020**, *21*, 481. [[CrossRef](#)]
78. Kaiser, J. Hormesis: Sipping from a poisoned chalice Science. *Science* **2003**, *302*, 376–379. [[CrossRef](#)]
79. Calabrese, E.J. Hormetic mechanisms. *Crit. Rev. Toxicol.* **2013**, *43*, 580–606. [[CrossRef](#)]
80. Proskurnina, E.V.; Mikheev, I.V.; Savinova, E.A.; Ershova, E.S.; Veiko, N.N.; Kameneva, L.V.; Dolgikh, O.A.; Rodionov, I.V.; Proskurnin, M.A.; Kostyuk, S.V. Effects of Aqueous Dispersions of C₆₀, C₇₀ and Gd@C₈₂ Fullerenes on Genes Involved in Oxidative Stress and Anti-Inflammatory Pathways. *Int. J. Mol. Sci.* **2021**, *22*, 6130. [[CrossRef](#)]
81. Mikheev, I.V.; Sozarukova, M.M.; Izmailov, D.Y.; Kareev, I.E.; Proskurnina, E.V.; Proskurnin, M.A. Antioxidant Potential of Aqueous Dispersions of Fullerenes C₆₀, C₇₀, and Gd@C₈₂. *Int. J. Mol. Sci.* **2021**, *22*, 5838. [[CrossRef](#)] [[PubMed](#)]
82. Mikheev, I.V.; Sozarukova, M.M.; Proskurnina, E.V.; Kareev, I.E.; Proskurnin, M.A. Non-Functionalized Fullerenes and Endo-fullerenes in Aqueous Dispersions as Superoxide Scavengers. *Molecules* **2020**, *25*, 2506. [[CrossRef](#)] [[PubMed](#)]

83. Fang, H.; Cong, H.; Suzuki, M.; Bao, L.; Yu, B.; Xie, Y.; Mizorogi, N.; Olmstead, M.M.; Balch, A.L.; Nagase, S.; et al. Regioselective Benzyl Radical Addition to an Open-Shell Cluster Metallofullerene. Crystallographic Studies of Cocrystallized $\text{Sc}_3\text{C}_2@I\text{h-C}_{80}$ and Its Singly Bonded Derivative. *J. Am. Chem. Soc.* **2014**, *136*, 10534–10540. [[CrossRef](#)] [[PubMed](#)]
84. Paiva, C.N.; Bozza, M.T. Are Reactive Oxygen Species Always Detrimental to Pathogens? *Antioxid. Redox Signal.* **2014**, *20*, 1000–1034. [[CrossRef](#)] [[PubMed](#)]
85. Herb, M.; Schramm, M. Functions of ROS in Macrophages and Antimicrobial Immunity. *Antioxidants* **2021**, *10*, 313. [[CrossRef](#)] [[PubMed](#)]
86. Remmel', N.N.; Titova, N.M.; Kratasyuk, V.A. Oxidative stress monitoring in biological samples by bioluminescent method. *Bull. Exp. Biol. Med.* **2003**, *136*, 209–211. [[CrossRef](#)]
87. Alexandrova, M.; Rozhko, T.; Vydryakova, G.; Kudryasheva, N. Effect of americium-241 on luminous bacteria. Role of peroxides. *J. Environ. Radioact.* **2011**, *102*, 407–411. [[CrossRef](#)]
88. Nemtseva, E.V.; Kudryasheva, N. The mechanism of electronic excitation in bacterial bioluminescent reaction. *Russ. Chem. Rev.* **2007**, *76*, 101–112. [[CrossRef](#)]
89. Lee, J.; Müller, F.; Visser, A.J.W.G. The sensitized bioluminescence mechanism of bacterial luciferase. *Photochem. Photobiol.* **2019**, *95*, 679–704. [[CrossRef](#)]
90. Weyemi, U.; Dupuy, C. The emerging role of ROS-generating NADPH oxidase NOX4 in DNA-damage responses. *Mutat. Res.* **2012**, *751*, 77–81. [[CrossRef](#)]
91. Sedelnikova, O.A.; Redon, C.E.; Dickey, J.S.; Nakamura, A.J.; Georgakilas, A.G.; Bonner, W.M. Role of oxidatively induced DNA lesions in human pathogenesis. *Mutat. Res.* **2010**, *704*, 152–159. [[CrossRef](#)] [[PubMed](#)]
92. Lambeth, J.D. Nox enzymes, ROS, and chronic disease: An example of antagonistic pleiotropy. *Free Radic. Biol. Med.* **2007**, *43*, 332–347. [[CrossRef](#)] [[PubMed](#)]
93. Zou, T.; Zhen, M.; Li, J.; Chen, D.; Feng, Y.; Li, R.; Wang, C. The effect of hemiketals on the relaxivity of endohedral gadofullerenols. *RSC Adv.* **2015**, *5*, 96253–96257. [[CrossRef](#)]
94. Kareev, I.V.; Bubnov, V.P.; Alidzhanov, E.K.; Pashkevich, S.N.; Lantukh, Y.D.; Letuta, S.N.; Razdobreev, D.A. Clustering of endohedral metallofullerenes with Y, Gd, Ho in solution and on the surface of a solid. *Solid State Phys.* **2016**, *58*, 1859. (In Russian) [[CrossRef](#)]
95. Bezmelnitsyn, V.N.; Yeletsky, A.V.; Okun, M.V. Fullerenes in solutions. *Successes Phys. Sci.* **1998**, *168*, 1195–1220. (In Russian)
96. Szpilewska, H.; Czyż, A.; Wgrzyn, G. Experimental Evidence for the Physiological Role of Bacterial Luciferase in the Protection of Cells Against Oxidative Stress. *Curr. Microbiol.* **2003**, *47*, 379–382. [[CrossRef](#)]
97. Wilson, T.; Hastings, J.W. Bioluminescence. *Annu. Rev. Cell. Dev. Biol.* **1998**, *14*, 197–230. [[CrossRef](#)]
98. Vetrova, E.V.; Kudryasheva, N.S.; Kratasyuk, V.A. Redox compounds influence on the NAD(P)H:FMN-oxidoreductase-luciferase bioluminescent system. *Photochem. Photobiol. Sci.* **2007**, *6*, 35–40. [[CrossRef](#)]
99. Vetrova, E.V.; Kudryasheva, N.S.; Visser, A.J.W.G.; Hoek, A. Characteristics of endogenous flavin fluorescence of *Photobacterium leiognathi* luciferase and *Vibrio fischeri* NAD(P)H:FMN-oxidoreductase. *Luminescence* **2005**, *20*, 205–209. [[CrossRef](#)]
100. Duan, W.; Meng, F.; Cui, H.; Linc, Y.; Wang, G.; Wu, J. Ecotoxicity of phenol and cresols to aquatic organisms. *Ecotoxicol. Environ. Saf.* **2018**, *157*, 441–456. [[CrossRef](#)]
101. Stasiuk, M.; Kozubek, A. Biological activity of phenolic lipids. *Cell. Mol. Life Sci.* **2010**, *67*, 841–860. [[CrossRef](#)] [[PubMed](#)]
102. Kamnev, A.A.; Kovács, K.; Kuzmann, E.; Vértes, A. Application of Mössbauer spectroscopy for studying chemical effects of environmental factors on microbial signalling: Redox processes involving iron(III) and some microbial autoinducer molecules. *J. Mol. Struct.* **2009**, *924–926*, 131–137. [[CrossRef](#)]
103. Kamnev, A.A.; Dykman, R.L.; Kovács, K.; Pankratov, A.N.; Tugarova, A.V.; Homonnay, Z.; Kuzmann, E. Redox interactions between structurally different alkylresorcinols and iron(III) in aqueous media: Frozen-solution ^{57}Fe Mössbauer spectroscopic studies, redox kinetics and quantum chemical evaluation of the alkylresorcinol reactivities. *Struct. Chem.* **2014**, *25*, 649–657. [[CrossRef](#)]
104. Goncharova, E.A.; Isakova, V.G.; Tomashevich, E.V.; Churilov, G.N. Obtaining of water-soluble polyhydroxylated fullereneols with iron nanoparticles as catalyzers. *Vestn. SibGAU* **2009**, *22*, 90–93. (In Russian)
105. Sun, D.; Huang, H.; Yang, S. Synthesis and characterization of a water-soluble endohedral metallofullerol. *Chem. Mater.* **1999**, *11*, 1003–1006. [[CrossRef](#)]
106. Isakova, V.G.; Goncharova, E.A.; Bayukov, O.A.; Churilov, G.N. Hydroxylation of fullerenes modified with iron nanoparticles. *Russ. J. Appl. Chem.* **2011**, *84*, 1165–1169. [[CrossRef](#)]
107. Churilov, G.; Popov, A.; Vnukova, N.; Dudnik, A.; Samoylova, N.; Glushenko, G. Controlled synthesis of fullerenes and endohedral metallofullerenes in high frequency arc discharge. *Fuller. Nanotub. Car. N.* **2016**, *24*, 675–678. [[CrossRef](#)]
108. Churilov, G.N.; Kratschmer, W.; Osipova, I.V.; Glushenko, G.A.; Vnukova, N.G.; Kolonenko, A.L.; Dudnik, A.I. Synthesis of fullerenes in a high-frequency arc plasma under elevated helium pressure. *Carbon* **2013**, *62*, 389–392. [[CrossRef](#)]
109. Churilov, G.N.; Popov, A.A.; Vnukova, N.G.; Dudnik, A.I.; Glushchenko, G.A.; Samoylova, N.A.; Dubinina, I.A.; Gulyaeva, U.E. A method and apparatus for high-throughput controlled synthesis of fullerenes and endohedral metal fullerenes. *Tech. Phys. Lett.* **2016**, *42*, 475–477. [[CrossRef](#)]
110. Akiyama, K.; Hamano, T.; Nakanishi, Y.; Takeuchi, E.; Noda, S.; Wang, Z.; Kubuki, S.; Shinohara, H. Non-HPLC rapid separation of metallofullerenes and empty cages with TiCl_4 Lewis acid. *J. Am. Chem. Soc.* **2012**, *134*, 9762–9767. [[CrossRef](#)]

111. Li, J.; Zhang, M.; Sun, B.; Xing, G.; Song, Y.; Guo, H.; Chang, Y.; Ge, Y.; Zhao, Y. Separation and purification of fullerenols for improved biocompatibility. *Carbon* **2012**, *50*, 460–469. [[CrossRef](#)]
112. Li, J.; Wang, T.; Feng, Y.; Zhang, Y.; Zhen, M.; Shu, C.; Jiang, L.; Wang, Y.; Wang, C. A water-soluble gadolinium metallofullerenol: Facile preparation, magnetic properties and magnetic resonance imaging application. *Dalton Trans.* **2016**, *45*, 8696–8699. [[CrossRef](#)] [[PubMed](#)]
113. Kuznetsov, A.M.; Rodicheva, E.K.; Shilova, E.V. Bioassay based on lyophilized bacteria. *Biotekhnologiya* **1996**, *9*, 57–61. (In Russian)
114. Fedorova, E.; Kudryasheva, N.; Kuznetsov, A.; Mogil'naya, O.; Stom, D. Bioluminescent monitoring of detoxification processes: Activity of humic substances in quinone solutions. *J. Photochem. Photobiol. B* **2007**, *88*, 131–136. [[CrossRef](#)] [[PubMed](#)]
115. Khan, P.; Idrees, D.; Moxley, M.A.; Corbett, J.A.; Ahmad, F.; von Figura, G.; Sly, W.S.; Waheed, A.; Hassan, M.I. Luminol-Based Chemiluminescent Signals: Clinical and Non-Clinical Application and Future Uses. *Appl. Biochem. Biotechnol.* **2014**, *173*, 333–355. [[CrossRef](#)] [[PubMed](#)]
116. Vasil'ev, R.F.; Veprintsev, T.L.; Dolmatova, L.S.; Naumov, V.V.; Trofimov, A.V.; Tsaplev, Y.B. Kinetics of Ethylbenzene Oxy-Chemiluminescence in the Presence of Antioxidants from Tissues of the Marine Invertebrate Eupentacta Fraudatrix: Estimating the Concentration and Reactivity of the Natural Antioxidants. *Kinet. Catal.* **2014**, *55*, 148–153. [[CrossRef](#)]
117. Gmurman, V.E. *Fundamentals of Probability Theory and Mathematical Statistics*; Berenblut, I.I., Ed.; Iliffe Book Ltd.: London, UK, 1968; p. 249.